10A
PLUMES DURING DISPOSAL (CAPITAL)

LYTTELTON HARBOUR/WHAKARAUPŌ CHANNEL DEEPENING PROJECT

Simulations of suspended sediment plumes generated from the deposition of spoil at the offshore disposal site

Prepared for Lyttelton Port Company Limited

PO Box 441, New Plymouth, New Zealand
T: 64-6-7585035 E: enquiries@metocean.co.nz

MetOcean Solutions Ltd: Report P0201-02

March 2016

Report status

Version	Date	Status	Approved by
RevA	18/03/2016	Updated draft for internal review	Weppe
RevB	27/03/2016	Updated draft for internal review	Beamsley
RevC	29/03/2016	Updated draft for internal review	Thiebaut
RevD	29/03/2016	Draft for client review	Beamsley
RevE	20/05/2016	Updated draft for internal review	Weppe
RevF	20/05/2016	Draft for client review	Beamsley
RevG	04/08/2016	Updated draft for client review	Beamsley
Rev0	21/09/2016	Approved for release	Beamsley

It is the responsibility of the reader to verify the currency of the version number of this report.

PO Box 441, New Plymouth, New Zealand
T: 64-6-7585035 E: enquiries@metocean.co.nz

TABLE OF CONTENTS

LIST OF FIGURES

LIST OF TABLES

1. INTRODUCTION

Lyttelton Port Company Limited (LPC) proposes deepening of the harbour shipping channel and turning basin to accommodate vessels with increased draughts, and disposing of the dredged material at an offshore site. A full description of the Channel Deepening Project (CDP) activities, location and methodologies is provided in Section Two (Project Description) of the associated Assessment of Environmental Effects (AEE), while Figure 1. provides an outline of the proposed deepened channel and capital disposal ground.

LPC has commissioned MetOcean Solutions Ltd (MSL) to undertake a numerical model study to investigate the dispersion of the passive plume associated with the discharge of sediment at the proposed offshore disposal ground from three different dredgers.

The discharge of dredge spoil occurs over a specific future period of time, but is inherently non-deterministic in that the dispersal and depositional outcomes are influenced by random variables such as currents and turbulence.

To account for this variability when making an assessment of the likely effects, simulations of the discharge over multi-year periods need to be undertaken so that robust statistical outcomes can be derived. In this process, the actual historical oceanographic conditions are recreated and then the disposal discharge is simulated over that period, creating a multi-year database with a range of seasonal and inter-annual outcomes that represent the natural variability.

For this study, the general characteristics of the plume dispersion were investigated by simulating disposal events during discrete time periods, with hydrodynamic and atmospheric forcing conditions typical of the disposal ground region. To produce robust probabilistic estimations of expected plume dispersion and deposition patterns, these short-term event-based simulations were supplemented by long-term numerical simulations of dredge spoil disposal over a 10-year period. Several reference sites were selected within the disposal ground extent to allow a characterisation of spatial variation of dispersion processes across the disposal ground. In reality, spoil is proposed to be spread throughout the disposal ground in order to both distribute the sediment around as evenly as possible within the disposal ground, and otherwise to managed disposal so as to minimise the potential excursion of associated plumes. A representative sediment grain size distribution based on the sediment expected to be dredged from the shipping channel was defined and used in the plume simulations.

The report is structured as follows; Section 2 details the numerical dispersal modelling methods that have been employed. The results are provided in Section 3 and a summary of the work is provided in Section 4. References cited are listed in the final Section.

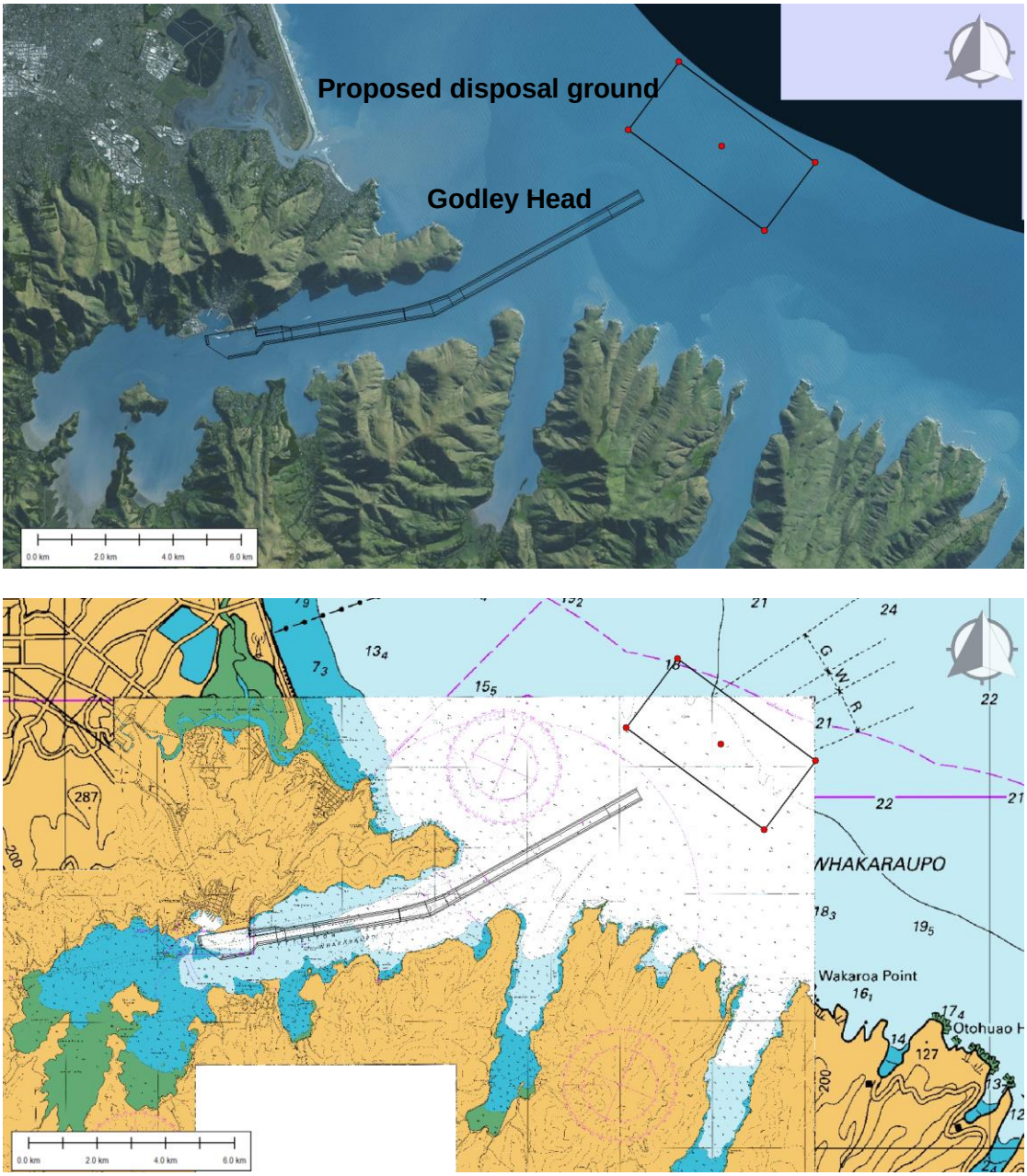

Figure 1.1 Footprints of the new proposed shipping channel and offshore disposal ground. Release sites considered in the disposal simulations are shown in red (see Table 2.1 for actual positions). Water depth throughout the ground is ~ 20 m.

2. METHODS

Modelling dredging plumes within a marine environment involves multiple steps with a brief and concise overview provided below. These steps required MSL to;

1. Develop, calibrate and validate a hydrodynamic model of the receiving environment that accurately captures the expected variability in the tidal and non-tidal current velocities.

2. Define source terms, including particle release points within the water column and percentages of the dredged material expected to be entrained into the passive plume.

3. Define representative fall velocities for the particles released within a numerical model framework and track these particles over time until they settle out of suspension.

4. Post-processing the results to add specific mass to these particles and undertake post processing of salient statistics that provide an overview of the expected plume characteristics.

Details of these steps are provided in the following sections

2.1. Approach

Two approaches are used to characterise of the passive plume dispersion resulting from the disposal operations, they are;

1. Modelling discrete disposal events, and

2. Modelling long-term simulations of disposal activities to statistically investigate the expected plume extents and characteristics.

Discrete disposal events were simulated at specific time periods (identified in a historical hindcast dataset) during which the hydrodynamic and atmospheric forcing conditions were representative of the expected range at the disposal site..

As the actual conditions during the discharge of dredge material for the proposed CDP are unknown, a second approach is also applied. This second approach consisted of running long-term simulations of disposal activities (10 year) within the historical context (in order to capture natural variability of the forcing conditions at the site). This enables robust probabilistic estimations of the spatial dispersion of the disposal plume and associated deposition patterns to be produced.

Plumes from representative sites within the proposed disposal ground (Figure 1.1, Table 2.1) are used to examine the expected spatial distribution of the plumes for both the discrete events and the long term simulation.

Table 2.1 Release sites. Co-ordinates are given in WGS84

	Longitude	Latitude
Site 1	172.869	-43.5563
Site 2	172.8875	-43.5383
Site 3	172.9187	-43.5832
Site 4	172.9372	-43.5651
Site 5	172.90313	-43.5607

2.2. Hydrodynamics

All the particle tracking simulations were undertaken using a 3-dimensional hydrodynamic hindcast simulated using the Regional Ocean Modelling System (ROMS) (Haidvogel, et al., 2000). A three-step nesting approach (see Figure 2.1) was employed starting from a New Zealand scale domain (0.08˚ resolution) and nested domains for the Central East of the South Island (0.03˚ resolution) and Pegasus Bay (0.003˚ resolution). Further details on ROMS, the model setup and validations are available in Soutelino and Beamsley (2015) and provided in Appendix A.

An example of the model output (monthly averaged residual current velocities) is given in Figure 2.2.

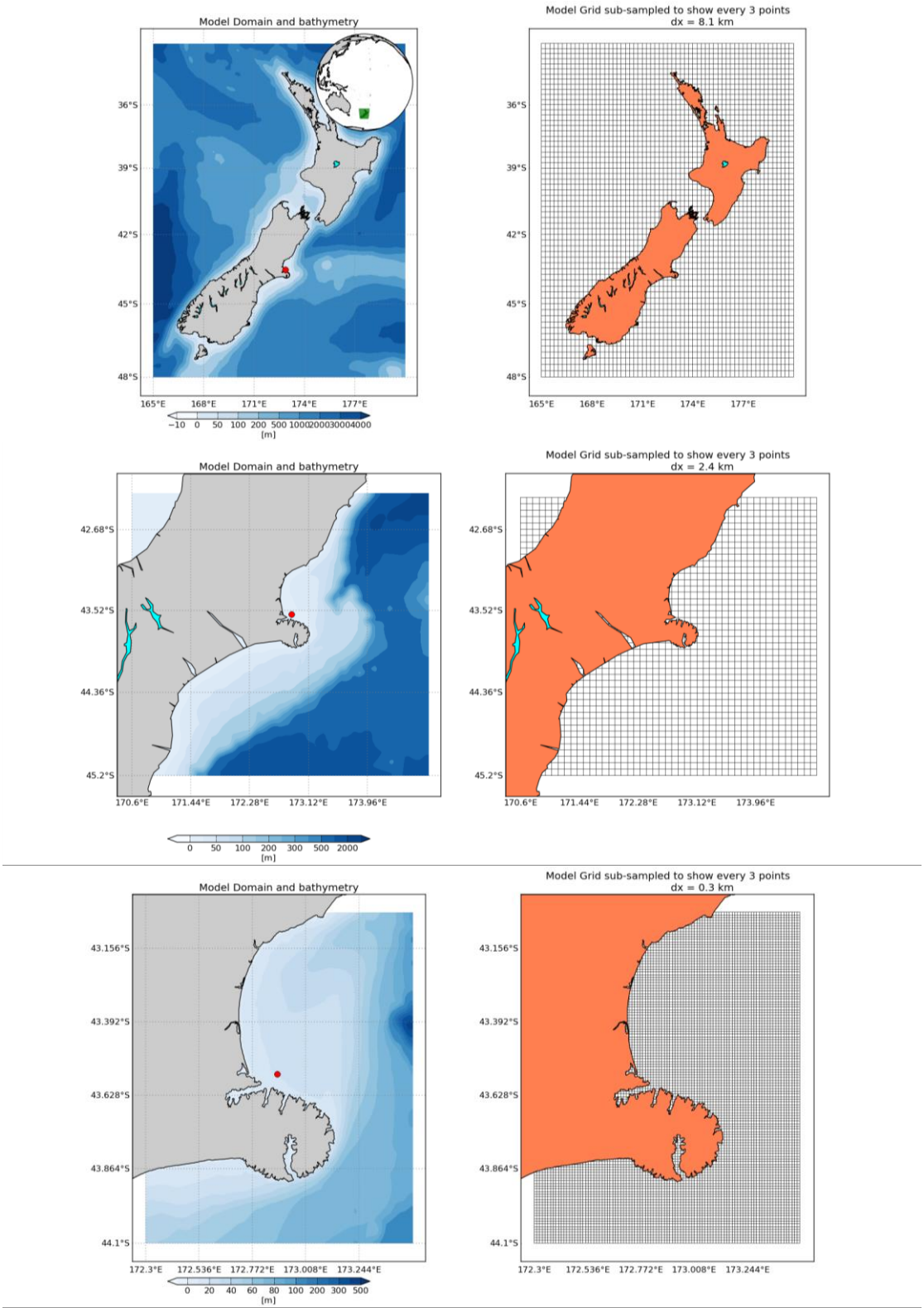

Figure 2.1 Hydrodynamical hindcast downscaling approach with ROMS. Upper panel shows the NZ 0.08˚ domain, middle panel shows the intermediate 0.03˚ Central East South Island (CESI) domain and lower panel shows the 0.003˚ PEGASUS domain. The right panel grids are showing every other 3 grid points, to allow easier graphical interpretation. Land mask is applied to the NW corner of CESI grid. The dot indicates the position from where current observations were used to validate the model results.

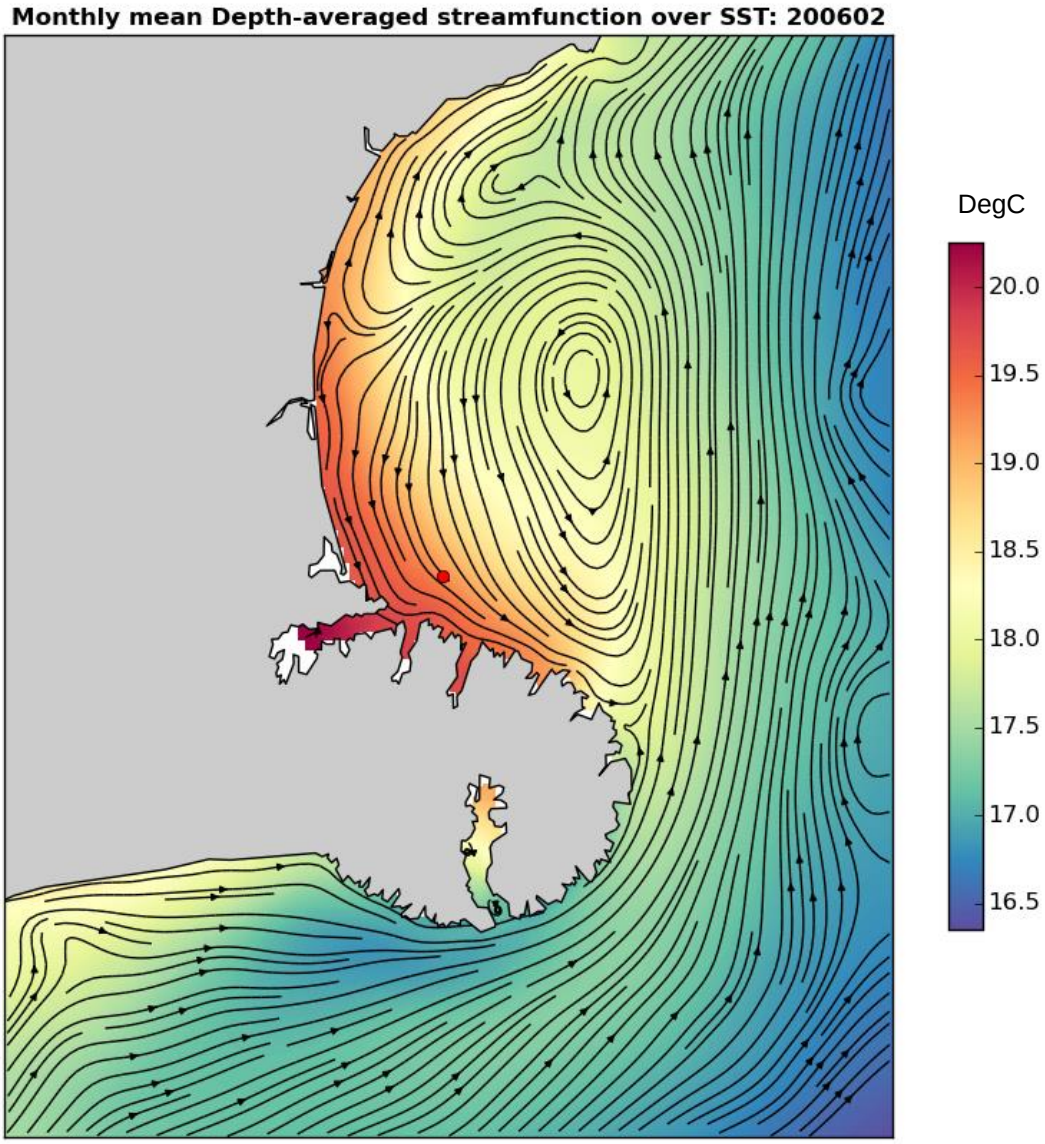

Figure 2.2 Monthly averaged residual flow for February 2006 for the ROMS Pegasus Bay, showing good agreement with literature-based flow features. The dot indicates the position from where current observations were used to validate the model results. Temperatures show the gradation from the cooler offshore waters within the Southland Current to the warmer waters that eddy in the lee of Banks Peninsular.

2.3. Trajectory Modelling

In order to understand how individual particles behave once released at the disposal ground, a Lagrangian model developed by MetOcean Solutions was used to simulate the trajectories of particles released at the different discharge points within the disposal ground. The model consists of a trajectory scheme applied to the existing ROMS 3D Eulerian current field $(\tilde{u},\tilde{v})$ solving for the motion of discrete particles:

$$\frac{dx_p}{dt} = \tilde{u}(x,y,z,t) + u_t$$
$$\frac{dy_p}{dt} = \tilde{v}(x,y,z,t) + v_t \qquad \text{(2.1 a,b,c)}$$
$$\frac{dz_p}{dt} = -w_s + w_g + w_t$$

where (u_t,v_t,w_t) are the diffusion components representing turbulent motions, w_s is the particle settling velocity and w_g is a vertical velocity component accounting for bathymetric gradients.

In the horizontal plane, the model uses an Ordinary Differential Equations (ODE) solver, including a 4th order Runge-Kutta method, to calculate the trajectory of a given particle (u_p,v_p) in the time-varying derivative field.

Diffusion is treated with the following equation, shown for the u_t component:

$$\int_t^{t+\Delta t} u_t . dt = \sqrt{6 . k_{u,v} . \Delta t} \; . \theta(-1,1) \qquad (2.2)$$

where $\theta(-1,1)$ is a random number from a uniform distribution between -1 and 1, Δt is the time step of the model in seconds and $k_{u,v}$ is the horizontal eddy diffusivity coefficient in $m^2.s^{-1}$.

In the absence of specific field data on diffusive processes, the determination of the diffusion coefficient $k_{u,v}$ is generally based on guidance from empirical relationships. Several relationships are summarized in Fischer et al. (1979) including that of Elder (1959) for simple unidirectional shear flows that estimates the longitudinal diffusion coefficient as a function of the water depth and current velocity of the form:

$$k_{u,v} = 5.93 . H . u^* \qquad (2.3)$$

where H and u^* are the water depth and friction velocity, respectively.

Transverse mixing can be estimated using a relationship of the same form but with reduced proportionality factor (with 50 % error bound):

$$k_{transverse} \sim 0.6 . H . u^* . \qquad (2.4)$$

The vertical diffusion is generally expected to be at least one order or magnitude smaller. Elder's formula suggests a vertically averaged value of: :

$$k_{vertical} \sim 0.067 . H . u^* . \qquad (2.5)$$

These equations can be used to provide a bracketing of reasonable diffusion coefficient values for the present application. Assuming a generic depth of 20 metres at the release site and a mean current velocity of 0.1 $m.s^{-1}$, the above equations yields coefficient in the range [0.35 - 0.5] $m^2.s^{-1}$, [0.04 - 0.05] $m^2.s^{-1}$, and ~0.005 $m^2.s^{-1}$ for the longitudinal, transverse and vertical diffusivities respectively.

Furthermore, in numerical models, the role of the horizontal diffusion coefficient is also to implicitly account for sub-grid scale turbulent processes such as eddies that are not explicitly resolved in the model due to the limited resolution. This means that horizontal diffusion must generally increase as grid size increases since eddies of increasing scale are unrepresented. Conversely, the reduction of grid size allows explicit resolution of flow patterns and eddies at finer scales, thereby reducing the required amount of added diffusion.

For dispersion at oceanic scales, Okubo (1971) notably showed that $k_{u,v}$ varies approximately (with wide scatter) as :

$$k_{u,v} = \alpha.L^{4/3} \tag{2.6}$$

where L is the horizontal scale of the mixing phenomena and α indicates proportionality.

Using a generic grid size of ~300 m for the Pegasus Bay model as a general length scale, the various diagrams provided in Okubo (1971) yield an horizontal diffusivity range of 0.1-1.0 $m^2.s^{-1}$.

Here, it was decided to take the average of the longitudinal and lateral diffusivities obtained with the Elder formula which yields ~0.2 $m^2.s^{-1}$.This value is consistent with the general order of magnitude provided by the Okubo equations. In general, the vertical diffusion should be at least two to three orders of magnitude smaller than horizontal diffusivities. Vertical diffusion is not expected to be the dominant process during the descent of the disposed sediment and a small generic value of 0.0001 $m^2.s^{-1}$ was used.

The trajectory of particles in the vertical plane is controlled by the particle's settling velocity w_s, the vertical diffusion component w_t as defined in equation 2.1c, and a component w_g related to the bathymetric gradient to ensure that the trajectory of a particle close to the sea-floor is parallel to it (before settling and diffusion components are applied):

$$w_g = \frac{(h-z)}{h}\left(\tilde{u}(x,y,z,t)\times\frac{dh}{dx}+\tilde{v}(x,y,z,t)\times\frac{dh}{dy}\right) \tag{2.7}$$

where z is the particle elevation above the seabed, h is the water-column height at the particles' horizontal location (x,y), $(\tilde{u},\tilde{v})$ is the 3D current field from equation 2.1 and $\left(\frac{dh}{dx},\frac{dh}{dy}\right)$ are the bathymetry gradients.

In the present model implementation, any particle reaching the shoreline, the seabed or the outside domain boundaries remained at the position of intersection (*i.e.* 'sticky' boundaries), thus allowing no sediment re-suspension. The mobility of deposited sediment is treated in a separate report.

2.4. Particle Size Distribution and Settling Velocity

The particle size distribution of the sediment to be dredged and disposed was estimated from sample data from the outer harbour presented in McLaren (2012). The surficial sediment consists of predominant fine material in the clay-silt range (0-63 µm) with a small fraction of fine sand (63 µm $<d_{50}<$256 µm) (see distribution in Figure 2.3).

For the simulations, the continuous sediment distribution was split into 4 discrete classes, each with a representative median grain size and dry sediment densities.

Although general equations are available to compute the settling velocity of individual particles of given sizes (e.g. Stokes Law), it is unrealistic to assume that the sediment consists in single particles in the fine silt range (~40 µm or smaller) because of the cohesive nature of material and associated flocculation effects (e.g. Van Rijn, 2007).

In the present application sediment smaller than 44 µm are assumed to belong to a single sediment class. In the absence of in-situ measurements on the settling of such flocculated cohesive sediment at the site, a generic settling rate of 1 $mm.s^{-1}$ was used, which is appropriate for such flocculated particles (Whitehouse et al., 2000), and commonly used in the context of sediment disposal (e.g. Smith and Friedrichs, 2011) to represent the finest sediment grain size fraction. The remaining sediment distribution was split into three additional classes with similar proportions, each with a representative median grain size computed as a weighted average from the continuous distribution. For these classes, particle settling velocities were computed using the standard equation of Van Rijn (1984) for non-cohesive sediment. Dry densities for the silt and sand material were set to 300 $kg.m^{-3}$ and 1600 $kg.m^{-3}$, respectively (Spearman, pers. comm.). The characteristics of the 4 representative classes and relative proportion of the total volumes are summarized in Table 2.2

Appropriate simulation time steps were chosen to correctly capture the horizontal trajectories due to the ambient tidal and residual flows. Time steps were also adjusted according to the particle settling velocities to ensure sufficient resolution of the vertical settling, and ranged from 60 to 600 seconds. The total number of particles released per time-step varied for each of the different size classes, to account for the different settling rates and to ensure a sufficient number of particles remained in suspension to account for the diffusion processes and to allow statistically representative concentrations to be derived. For example, a larger number of coarse silt particles were released per discharge event compared to the fine silts since a greater proportion of the coarse silt would settle over a given time period due to the higher settling velocities. Each sediment fraction is simulated separately and all results are combined afterwards to produce total suspended sediment concentration (*SSC*) fields.

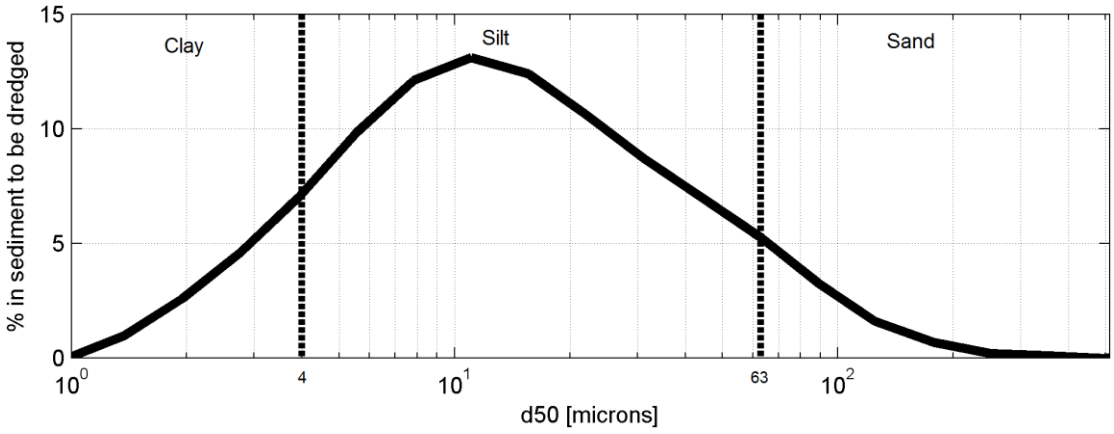

Figure 2.3 Particle size distribution of sediment to be dredged in the Lyttelton Harbour/Whakaraupō. The vertical dashed lines indicate the clay, silt, and sand size ranges.

Table 2.2 Representative median grain sizes, settling velocities, and proportions of total volume released for the 4 discrete classes.

	Representative d50 [microns]	**Settling velocity [m/s]**	**Percentage of total volume [%]**
Class 1	Smaller than 44.0	0.0010	81.8
Class 2	44.0	0.0014	7.0
Class 3	62.5	0.0028	5.3
Class 4	118.0	0.0085	5.9

2.5. Disposal scenarios

2.5.1. Sources terms

The processes by which sediment is released and suspended in the water column during disposal operations are briefly outlined here in the context of the choice of the source term magnitudes and release depths for the particle tracking simulations.

In the case of silt to fine sand dredging, the content of loaded dredgers consists of a highly concentrated mixture of sediment and water and the bulk behaviour of that sediment mixture becomes dominant over the individual particle settling processes. When the dredge opens its bottom door for release, the content will typically be released as a jet-like sediment flux quickly descending to the seabed. The behaviour of the released sediment can be separated in three main phases: 1) Convective descent, 2) Dynamic Collapse, and 3) Passive dispersion (Figure 2.4).

During the convective descent, the dense sediment material quickly descends to the bottom. Ambient water can become entrained around the perimeter of the jet which can strip, or de-entrained, some sediment that eventually becomes suspended in the water column. The proportion lost is expected to be small, commonly cited as 1-5 % of the disposed load (Bokuniewicz et al., 1978; Bokuniewicz et Gordon, 1980; Gordon, 1974; Truitt, 1988).

Following its descent, the dredge material collapses on impact with the seabed; this phase is known as the Dynamic Collapse phase. Note mid column collapse can occur in the specific case of a layer of density similar to that of the descending material. This is not expected to occur in the present case (Spearman, pers. comm.). The collapse results in a large fraction of the disposed sediment depositing on the seabed and is often coupled to the generation of the density current generated by the excess energy available following collapsing, whereby a fraction of the disposed sediment is suspended and propagates radially from the point of impact. The density current is expected to be contained within the bottom 15-20% of the water column, with excursion length scales of order 100-500 m (e.g. Aarninkhof and Luijendijk, 2009).

These two initial phases relating to the dissipation of the initial plume momentum are also referred to as dynamic plume stage (e.g. Spearman et al., 2007). The Passive dispersion phase relates to the subsequent dispersion of the sediment that became suspended in the water column during the dynamic phase, i.e. de-entrained during descent, and sediment suspension by the density current developing near the seabed by the ambient current.

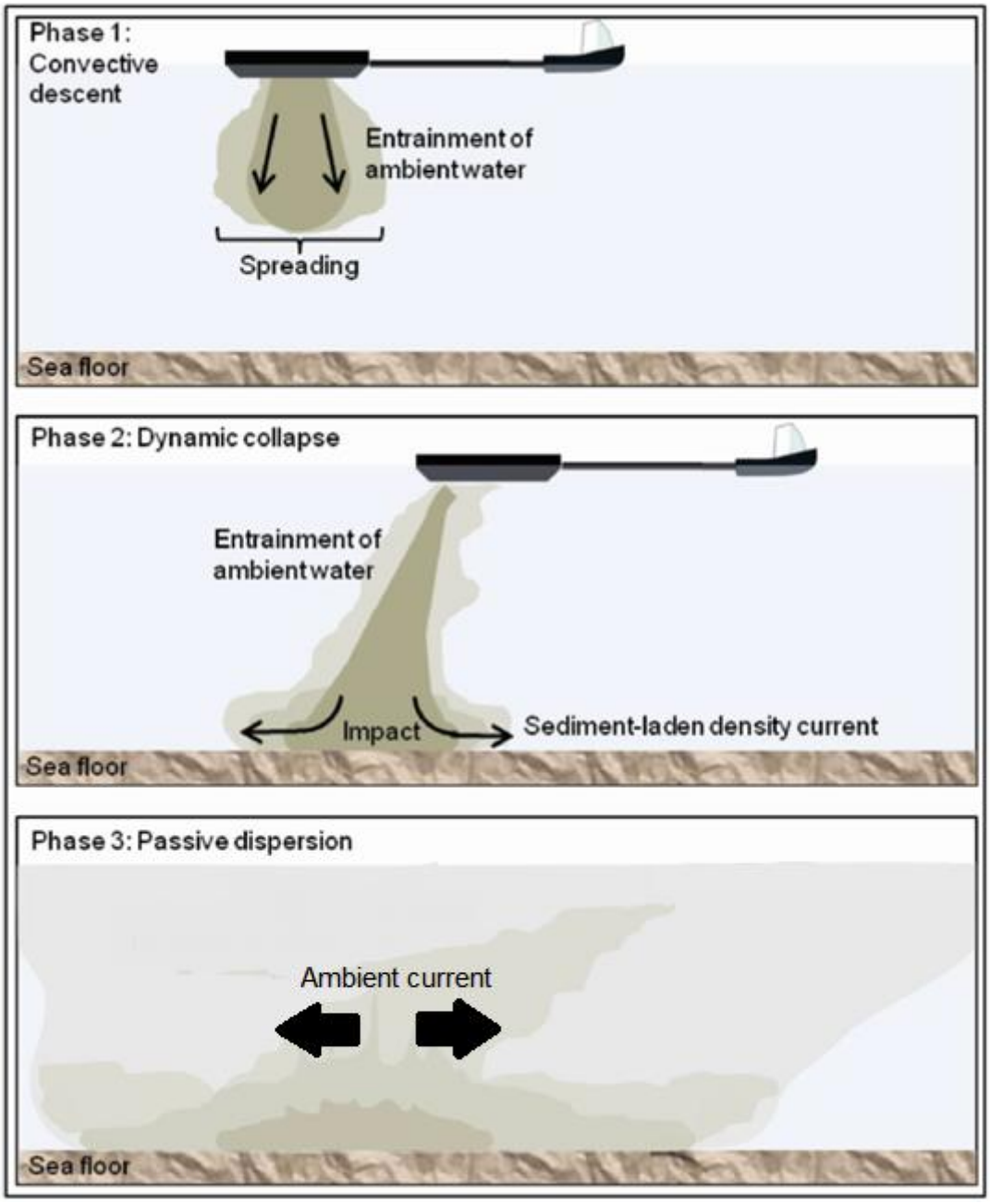

Figure 2.4 Three main phases occurring during the disposal of dredged material: 1) Convective descent, 2) Dynamic Collapse, and 3) Passive plume dispersion.

In the present study, the focus is on characterising the extents and concentrations of the plume resulting from this passive dispersion phase, as these plumes have the potential to effect order of magnitude greater spatial extents than the dynamic plume (which settles quickly). In that respect, the particle tracking simulations considered two main source terms:

- A) de-entrained sediment during descent – release at the bottom of the vessel used for disposal as a point source.
- B) Density current at the bottom - release within a cylinder near the seabed of given height and radius.

Note a degree of conservatism is introduced in the modelling by releasing the sediment stripped from the descending plume at the vessel bottom rather than throughout the water column. This results in the modelled

sediment remaining in suspension longer as the particles have further to fall (i.e. from the vessel bottom).

The present application also considered an additional sediment source released at near-surface, representative of sediment which, in the unlikely event, is entrained vertically around the hull of the dredger due to turbulence associated with the discharge of sediment.

- C) Surface sediment losses - release within the top layer of the water column (from the sea surface to bottom of vessel hull)

Simulations of near-field plume behaviour at the disposal site under realistic residual and tidal currents indicated that near-bed source terms should include 21% of the disposed sediment, distributed over a circular area of 300 m radius and 2 m height (Spearman, pers. comm.). This was combined with the mid-water and near surface release source terms (i.e. de-entrained and surface loss) which were assumed to consist of 5% and 1% of the disposed load respectively (see Figure 2.5).

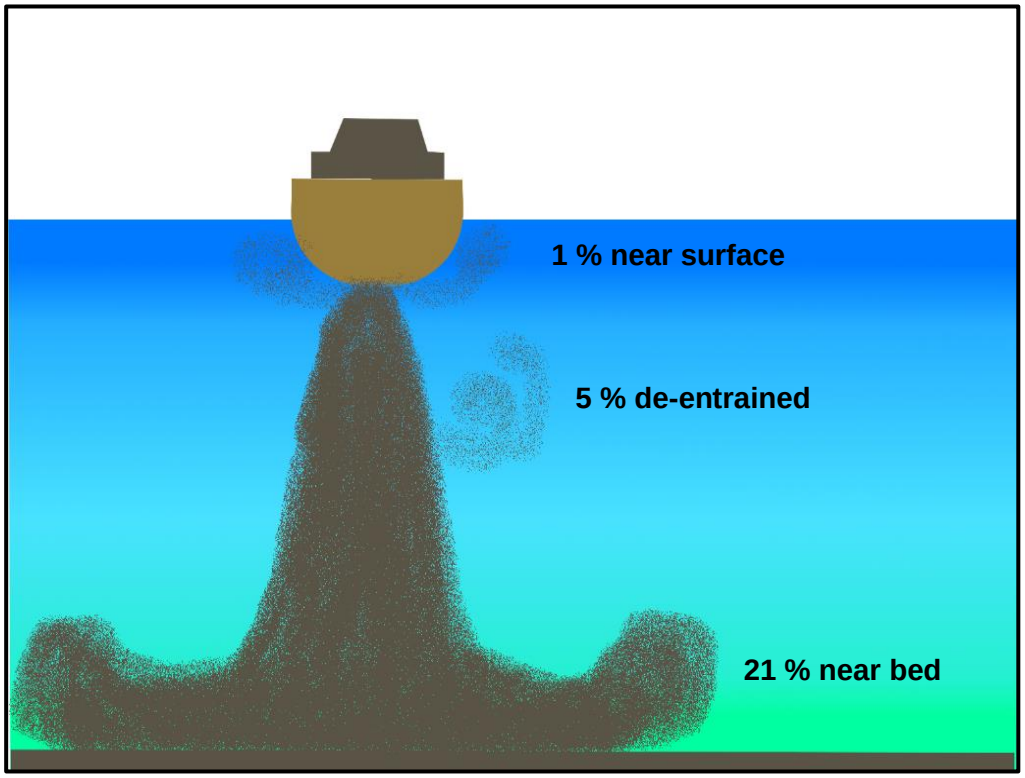

Figure 2.5 Percentages of sediment transferred from the near-field density driven plume to the far-field plume.

The near-bed source term was defined by dedicated model simulations. However, it is stressed that the use of ratios for the proportions of sediment involved transferred in the passive plumes due to stripping during descent and other losses near the surface (i.e. 5 and 1 % respectively) is a relatively simplistic approach. Sensitivity testing of the ratio suggests it does not significantly alter the predicted *SSC* magnitudes, particularly in the surface layer and it was decided to use 5% values for conservatism. The repartition of the disposal load volume within the different sources is illustrated in Figure 2.6.

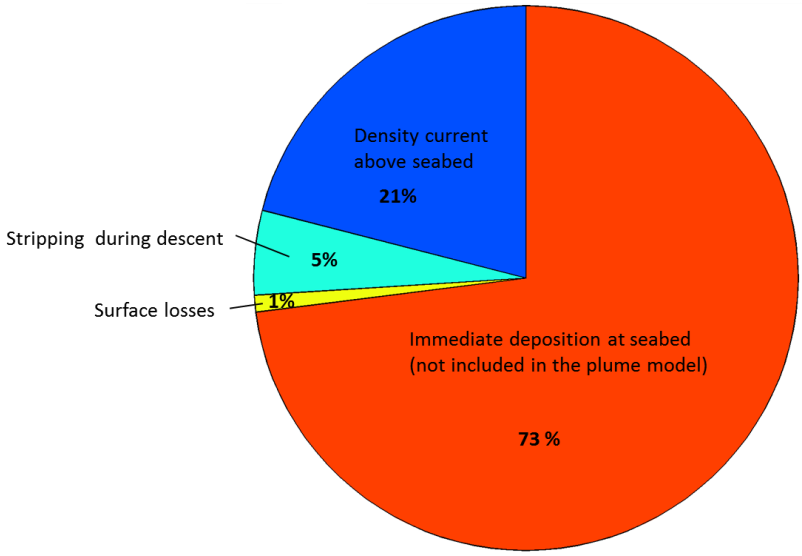

Figure 2.6 Repartition of the hopper load volume within the different source terms considered in the simulations.

The release depths for the source terms and total disposed volumes were varied based on the example dredgers likely to be used for the dredging and disposal operations. To consider the spatial variability of the future disposals, releases were simulated at the centre and corners of the proposed disposal ground (Figure 1.1). Positions are provided in Table 2.1 and details of the dredging vessels are summarized in Table 2.3 and associated source terms are given in Table 2.4

.

Table 2.3 Details of the dredging vessels likely to be used for dredging and disposal works.

Vessel	Hopper load [m3]	Draught [m]	Disposal cycle [hours]
Asia	10,800	-9.5	2
Utrecht	18,000	-10.5	2
Olympia	5,000	-7.5	2

Table 2.4 Source terms and release depths.

Sources Terms	Percent of hopper volume	Release depth	Release type
Surface losses	1%	sea-surface to vessel draught	point source
De-entrained during descent	5%	vessel draught	point source
Density current	21%	2 m layer above seabed	300 m radius circle

2.5.2. Disposal events simulated

The dispersion model was run for a range of discrete disposal events during which the hydrodynamic and atmospheric forcing conditions were representative of the expected range at the disposal site, including both strong wind and ambient current events, and more ambient conditions (e.g. during calm conditions) in order to examine the potential maximum *SSC* in the vicinity of the disposal site (i.e. limiting the excursion extent of consecutive discharges).

In addition to the discrete short-term simulations, two 1-month periods during summer and winter months (January and August) were modelled. All events were identified during the 2010 year (see Figure 2.7, Table 2.5)

For the real-time simulations of disposal events, disposal events were simulated at 2-hourly interval to reproduce the expected filling and travel cycles.

The long-term simulations of the plume dispersion during the 10 year hydrodynamic hindcast assumed continuous release of sediment throughout the period in order to examine the potential dispersion of the plumes from a more statistical basis.

Simulating plumes from the near-bed, near-surface and de-entrained from the dynamic phase of the plume descent for each of the representative grain sizes (Section 2.4), while computationally demanding, provides the necessary information to derive representative statistical measures of the predicted plume extents for the range of climatic variability expected at the site.

Table 2.5 Summary of simulation periods

Disposal simulations	Period
Strong southeast-directed current	07/06/2010-12:30
Strong northwest-directed current	01/08/2010-12:30
Large northeast wind/wave event	12/05/2010-18:30
Calm period	11/02/2010 0:00
January & August months (summer/winter)	01/2010 and 08/2010
10 year hindcast	2003-2012

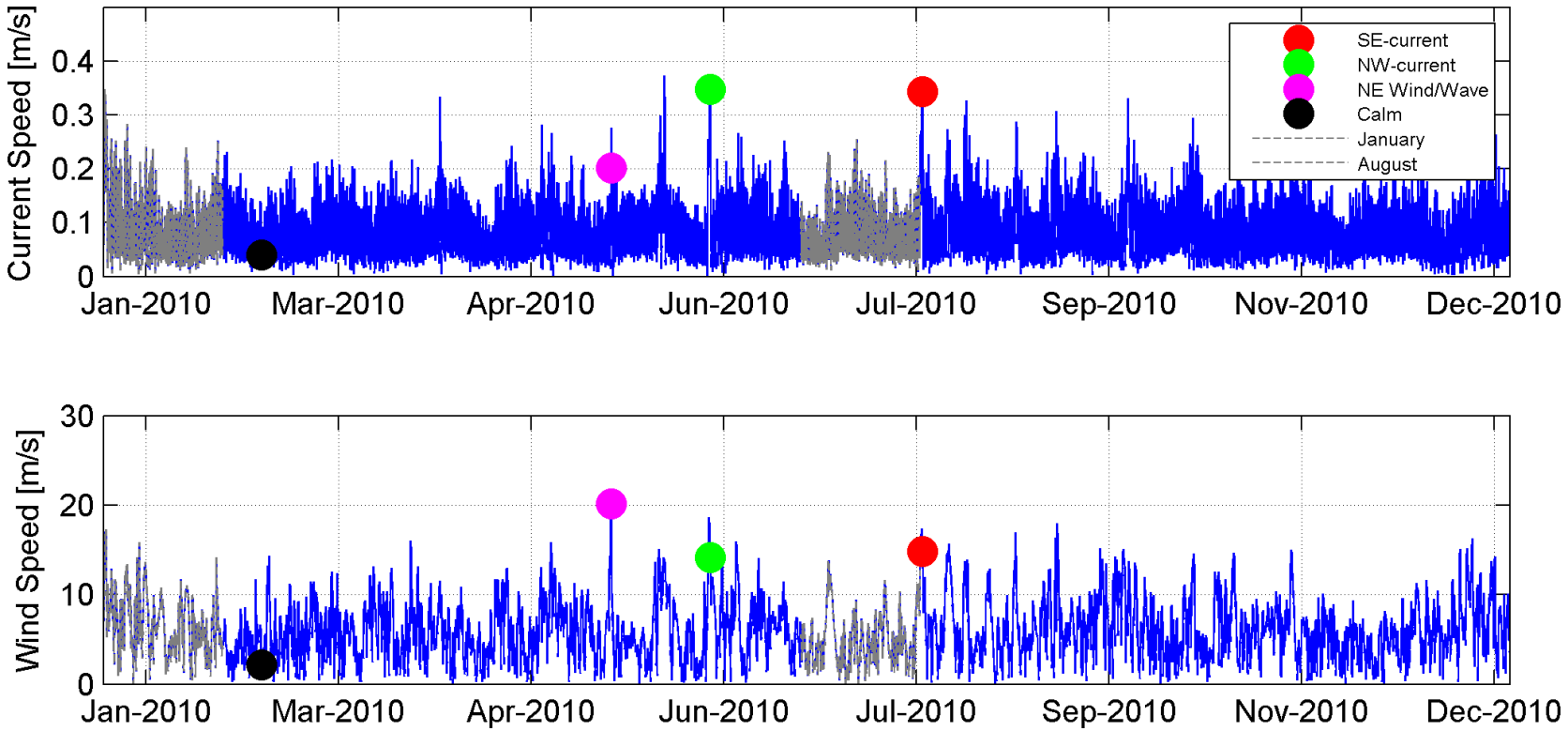

Figure 2.7 Time series of current and wind speed at the centre of the disposal site during 2010. The simulations periods are indicated as coloured dots and dashed lines. Coloured circles and greyed time-series lines show the discrete event simulated, as given in Table 2.5

2.6. Post-Processing

The general methods used to reconstruct concentration and deposition fields from the model outputs are outlined below.

2.6.1. Concentration and depositional thickness computation

To reconstruct concentrations from the particle tracking simulations at chosen receptors, a kernel method with variable bandwidth was used. The use of a variable bandwidth (kernel size) attempts to represent true variability of spatial concentration, while minimizing statistical variability that inevitably occurs away from the source, due to a necessarily finite number of particles. A small kernel is used in regions gathering a high number of particles, where it is statistically appropriate to infer relatively small scale changes in concentration. Conversely, a larger kernel is used in regions presenting a low number of particles, so as to prevent unrealistically high concentrations around the precise (but partially random) locations of a few isolated particles.

In practice, the concentration C at a given receptor location (x,y) is computed as:

$$C(x,y) = \sum_{i=1}^{n} \frac{m_i}{\lambda_x(x,y)\lambda_y(x,y)} K\left(\left|\frac{x_i - x}{\lambda_x}\right|\right) K\left(\left|\frac{y_i - y}{\lambda_y}\right|\right) \tag{2.8}$$

where (x_i,y_i) is the location of each particle i, n is the total number of particles, m_i is the loading for each particle, λ_x and λ_y are the kernel bandwidth in the x and y directions for location (x,y) and K is the kernel function.

Following Vitali et al. (2006), an Epanechnikov kernel function was used:

$$K(q) = \begin{cases} 0.75\left(1-q^2\right), |q| \le 1 \\ 0, |q| > 1 \end{cases} \tag{2.9}$$

where q is the ratio of the particle distance from receptor to bandwidth ($q_x=d_x/\lambda_x$, or $q_y=d_y/\lambda_y$)

A receptor-based method derived from the *RL3* method in Vitali et al. (2006) was used to define the bandwidths λ_x and λ_y.

For each receptor location, a neighborhood was defined as the region enclosing the 1/20th closest particles. Then, for each direction x and y, the bandwidths λ_x and λ_y were defined as the minimum value between the maximum projected distance of the particles within the neighborhood and twice the standard deviation of the projected distances within the neighborhood. Finally, in order to prevent unrealistically elongated kernels, the aspect ratio λ_x/λ_y was limited to be no greater than 5:1, with the smaller value increased.

The loading of each particle m_i directly depends on the quantity being modelled. Here, each discrete particle was attributed to a certain sediment mass which was determined as the ratio of the total sediment mass of a

given class per disposal load to the number of particles of that class released in the model at each disposal event.

The concentration measurement *C* in equation 2.8 yields depth independent concentration estimates in m^{-2}. Volume concentrations (in $kg.m^{-3}$) are obtained by implementing equation 2.5 within defined depth-bands. For this study, concentrations were estimated near the surface, mid-water and near-bed by limiting the concentration calculations to particles within a 4 m band relative to each of the levels.

Quantitative estimates of the probable depositional thickness where obtained by multiplying the probability densities of settled particles of each sediment class at a given receptor by their respective fraction within the disposed volumes, and then summing the contribution of each class:

$$D(x,y) = \sum_d \sum_i k_i V_d C_{d,i}(x,y) = \sum_d k V_d \sum_i C_{d,i}(x,y) \quad (2.10)$$

where $D(x,y)$ is the depositional thickness at the grid node location (x,y), V_d is the total discharged volume, k_i is the fraction of total volume for the sediment class *i* (see Table 2.2) and $C_{d,i}(x,y)$ is the settled particle probability density at location (x,y) for the sediment class *i*.

2.6.2. Application to the present study

In the present study, a range of different outputs are produced including:

- Successive concentration fields following the disposal of one hopper load during events with representative forcing conditions.
- Successive concentration fields following the disposal of three consecutive hopper loads at the same position during calm conditions (i.e. worst case scenario for concentration at the release site)
- Mean probabilistic suspended sediment concentrations (*SSC*) at three levels in the water column (surface, mid-water and near-bed) and mean deposition field resulting from the disposal activities, derived from the 10 year sediment disposal hindcast.
- Maps illustrating the percentage of time given *SSC* level thresholds are exceeded for the discrete events and during summer and winter months.
- Extreme particle excursion contours to provide a picture of the absolute worst case scenario of particle dispersion.

Results are based on suspended sediment concentrations (*SSC*) and deposition fields computed following the methodology presented in Section 2.6.1; with concentrations derived per sediment size class combined to produce total suspended sediment concentrations within the surface, mid-water and bottom layers, as well as deposition magnitudes. The grids used

for the computation of concentrations fields had elements size ranging from ~300 m offshore to ~25 m in the near vicinity of the disposal.

It is noted that the simulated suspended sediment concentrations should be interpreted as disposal-related *SSC* only, and would add to the ambient *SSC*.

2.7. Ambient suspended sediment concentrations

Limited information on the ambient *SSC* within the Lyttelton/Pegasus Bay environs is available at present, however sporadic *SSC* measurements (i.e. of the order 10 or less per year between 2003 and 2014) at 8 locations in and around Pegasus Bay and Lyttelton Harbour/Whakaraupō provide some guidance regarding the expected surface *SSC* within the receiving environment (Figure 2.8, Table 2.6).

The measured suspended sediment concentration range is similar to those observed in other coastal receiving environments around NZ, including south Taranaki (2-18 $mg.L^{-1}$ - Pinkerton et al., 2013; Zhou, 2012) and Hawke's Bay (< 50 $mg.L^{-1}$, Madarasz, 2006), and are several orders of magnitude less than the estimated average surface water *SSC* at the mouth of the Waimakariri River (estimated to be an average *SSC* of 1400 $mg.L^{-1}$, rising to $2.1x10^5$ $mg.L^{-1}$ during flooding events - Mulder and Syvitski, 1995, Figure 2.9).

Table 2.6 Suspended sediment concentration measurement locations. The mean and maximum *SSC* are given in $mg.L^{-1}$. Data provided by Environment Canterbury

Site	Easting	Northing	Mean *SSC* ($mg.L^{-1}$)	Max *SSC* ($mg.L^{-1}$)
Akaroa Harbour between Heads	1596874	5140017	11	41
Offshore Amberley Beach	1584499	5217827	11	31
Offshore Ashley River mouth	1580515	5207191	11	46
Offshore Waimakariri river mouth	1579695	5195459	14	34
Offshore New Brighton pier	1581149	5183852	11	39
Lyttelton Port entrance	1577117	5171475	17	110
Lyttelton Harbour/Whakaraupō	1584694	5172392	13	38
Lyttelton Harbour/Whakaraupō Midway	1579666	5171192	18	42

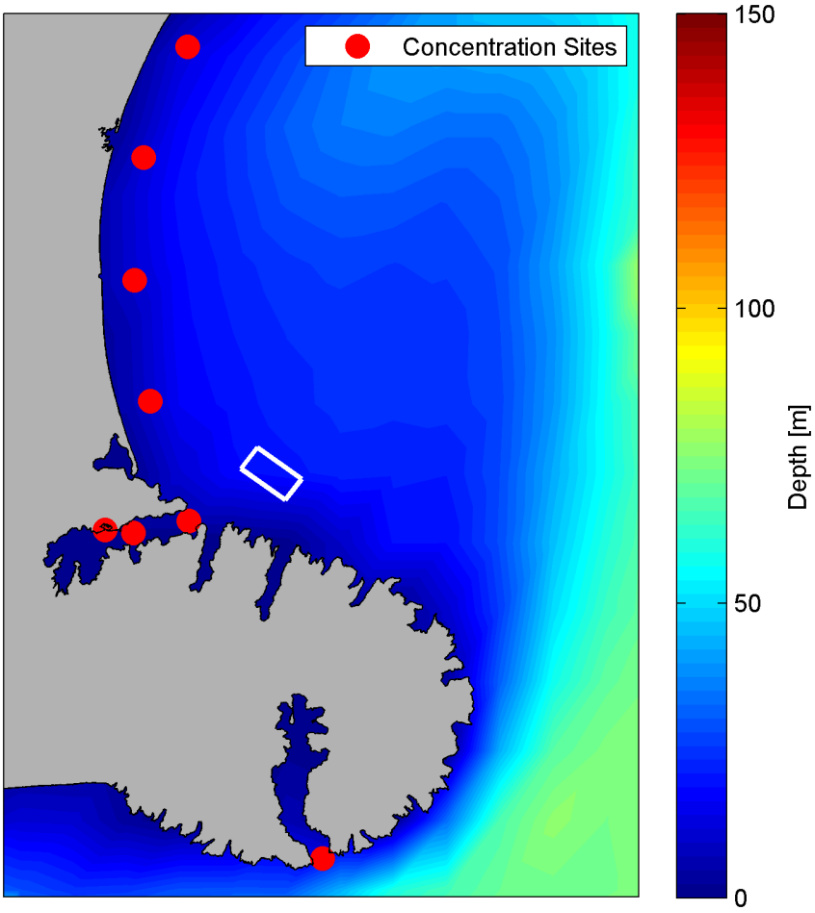

Figure 2.8 Mean suspended sediment concentrations based on limited surface measurements of *SSC* within the Lyttelton Harbour/Whakaraupō / Pegasus Bay environs.

Figure 2.9 Aerial image of sediment plume from the Waimakariri River during flood conditions.

3. RESULTS

This section presents the key results of the various simulations of sediment disposal at the offshore disposal ground.

The first section 3.1 outlines the sequential plume dispersion patterns following disposal under typical forcing conditions at the site.

The probabilistic estimations of the mean *SSC* plume and deposition footprints derived from the 10-year hindcast simulations are described in the second section 3.2.

The third section 3.3 includes estimations of percentage of time several key *SSC* thresholds are exceeded during typical summer and winter periods. These estimates can be used for ecological impact assessment.

Although simulations have been undertaken for three potential vessels, at all release sites, the Volvox Asia vessel with intermediate hopper load capacity is used as base case. The modulations of predicted *SSC* plumes and depositions patterns and magnitudes due to the use of other vessels are described for a release at the centre of the ground.

3.1. Disposal plumes during typical events

As a first approach, discrete disposal events were simulated during time periods subject to hydrodynamic and atmospheric forcing typical of the site. Predicted *SSC* plume dispersions during a 60-minute window are included in Figure 3.1 to Figure 3.3 for events with strong northwest current, strong southeast current and strong northeast wind and waves, respectively. The 60-minute window allows sufficient time for the majority of the disposed sediment to settle out of suspension.

The disposal of the hopper load initially results in relatively large *SSC* levels in the bottom layer that are associated with the density current, driven by the dynamic collapse of the dense sediment jet at the seabed (see Figure 2.4). The bottom *SSC* plume spreads within a circular radius of ~300 m as prescribed by the near-field modelling undertaken by HR Wallingford (Spearman pers. comm.) and is expected to initially consist of 21 % of the total hopper volume. The smaller and more compact *SSC* plumes in the mid-water and surface layers are associated with the de-entrainment of sediment from the dynamic plume during the descent of dense sediment “jet” (~5 % of total hopper volume) and losses near the surface (1%).

The sediment that is suspended in the water column through this initial phase is then subject to advection by the ambient currents, as well as diffusion (i.e. passive dispersion phase, see Figure 2.4). In all three cases, dispersion directions are consistent with the ambient current forcing. In the bottom layer, the *SSC* plume is driven by the near-bed currents but sediment will deposit relatively quickly given the proximity to the seabed. In general, during these energetic events, most of the circular near-bed *SSC* component of the passive plume will settle within 500 metres of the release site in the 30-45 minutes following disposal. After 45 minutes the *SSC* plumes are very compact in the three depth layers and essentially consist of the residual suspended sediment that settled from the surface to mid-water

layers or from the mid-water to bottom layer. The concentration fields at 120 and 180 minutes show no significant *SSC* plumes in the surface or mid-water layers with only very limited *SSC* patches in the bottom layer due to settling from the upper levels.

While dispersion during energetic events provide insights of the largest potential plume dispersions, simulations of sediment disposal during calm conditions can be used to examine the potential maximum *SSC* in the vicinity of the disposal site (i.e. limiting the excursion extent of consecutive discharges).

To provide a picture of the absolute worst case scenario with respect to the possible *SSC* levels in the ground vicinity, three successive hopper load disposals at the same site were simulated during calm conditions (current speed less than 0.05 $m.s^{-1}$ and wind speed less than 10 knots) (Figure 3.4 to Figure 3.6). A disposal cycle of two hours was simulated with actual disposal events occurring at 0, 120 and 240 minutes (i.e. top plots in Figure 3.4 to Figure 3.6).

Overall dispersion distances are expectedly increased relative to the strength of the current events. As mentioned above, the majority of the initial bottom *SSC* plume settle to the seabed within ~30 minutes. *SSC* levels in the bottom layers are then sequentially increased during transfer of suspended sediment from the surface and mid-depth layers (e.g. after 90 minutes) to the bottom layer, or the next disposal event (e.g. after 120 minutes). *SSC* plumes in the surface and mid-depth layers are initially very compact and relatively spread as they settle within the water column due to advection as well as diffusive processes.

The *SSC* plumes with the most significant extents and concentration magnitudes are consistently found in the bottom layer. However, the present simulations suggests that even under very unfavourable disposal conditions (i.e. low dispersion potential and same disposal site), *SSC* levels will typical drop below 100-200 $mg.L^{-1}$ within 1 km of the disposal location.

Northwest Current

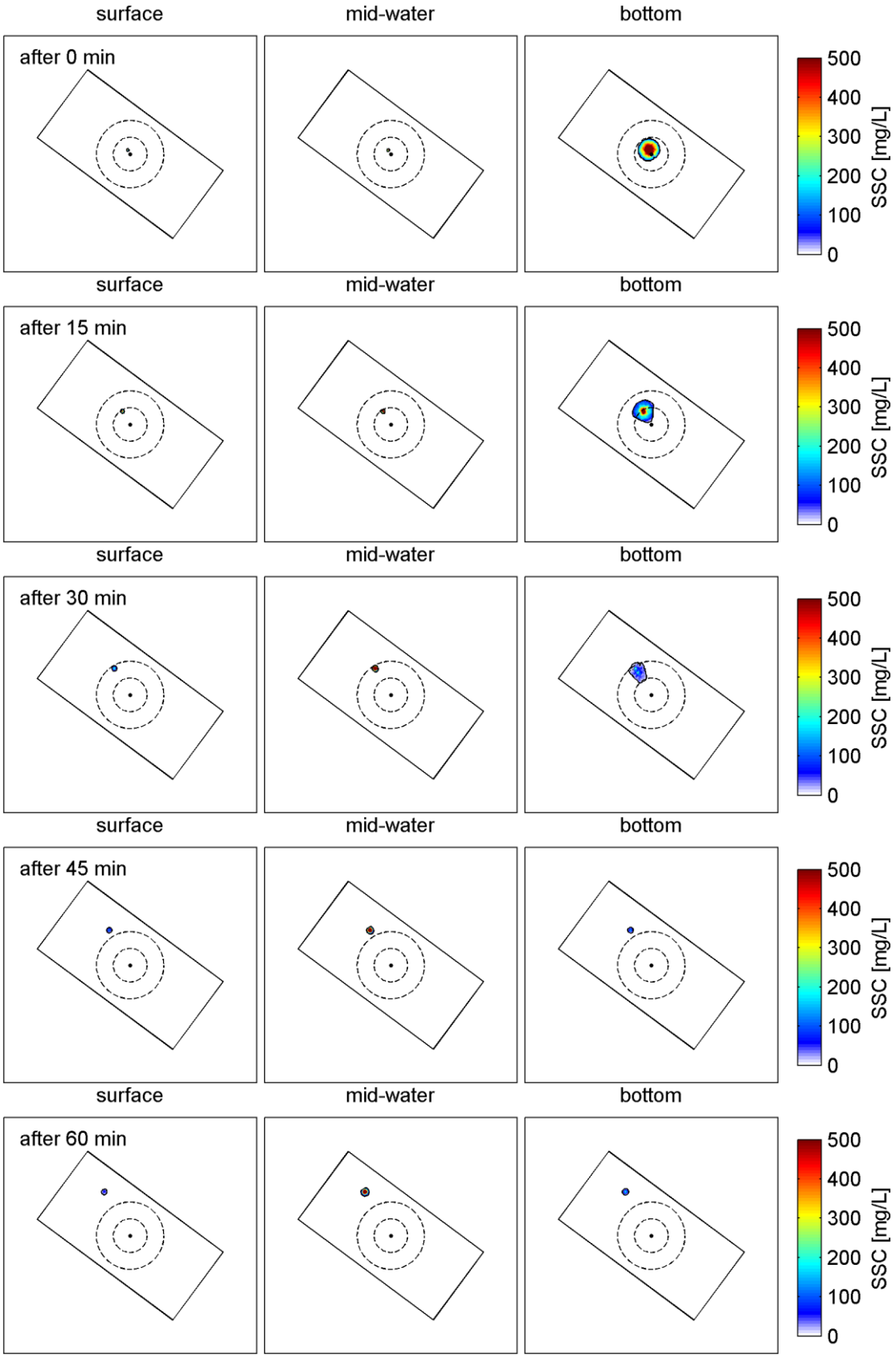

Figure 3.1 Disposal of one load of the Volvox Asia vessel (V=10,800 m^3) at site 5 during strong northwest currents. Dashed circles have radiuses of 500 and 1000 m.

Southeast current

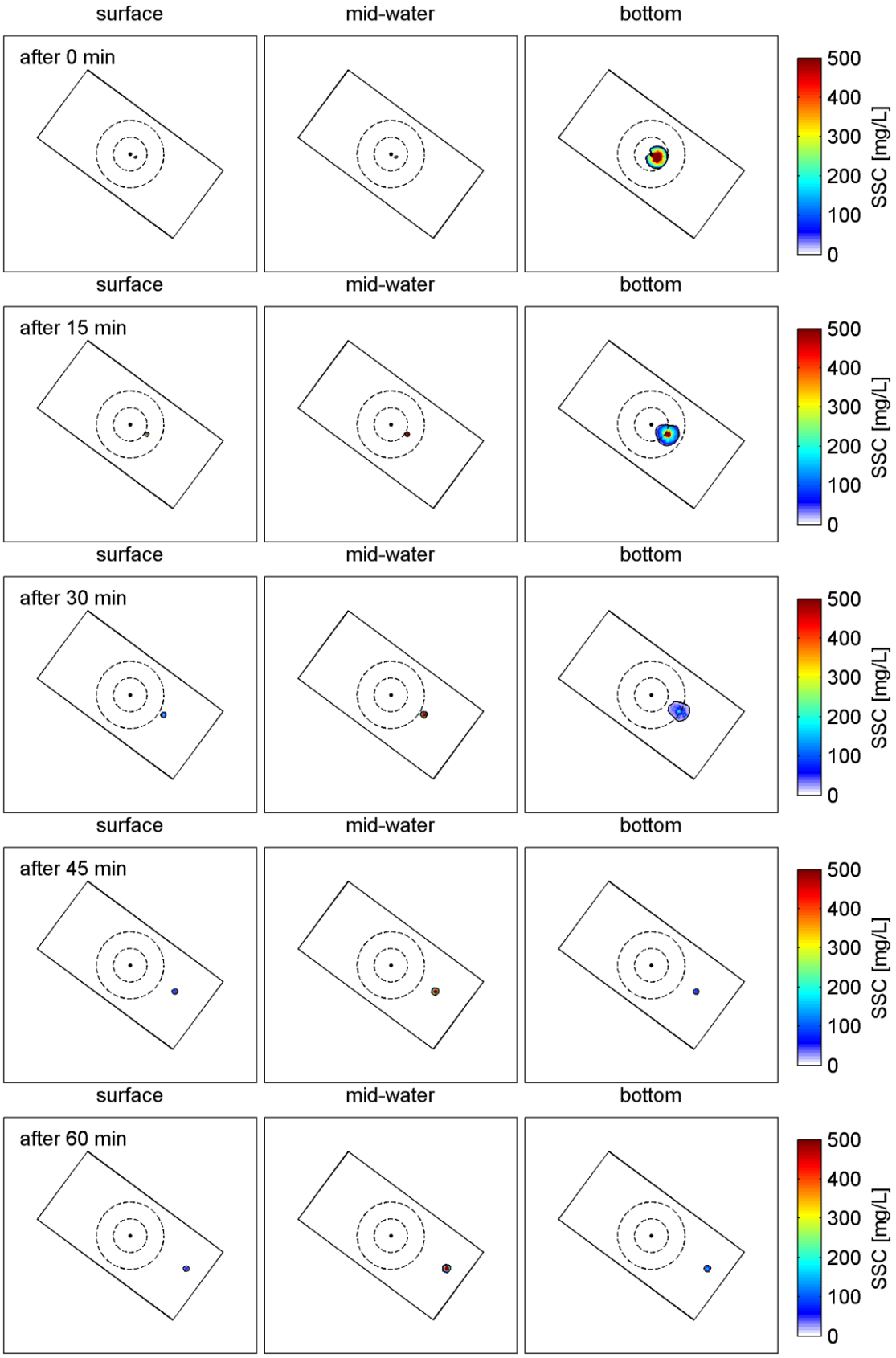

Figure 3.2 Disposal of one load of the Volvox Asia vessel (V=10,800 m^3) at site 5 during strong southeast currents. Dashed circles have radiuses of 500 and 1000 m.

Northeast winds

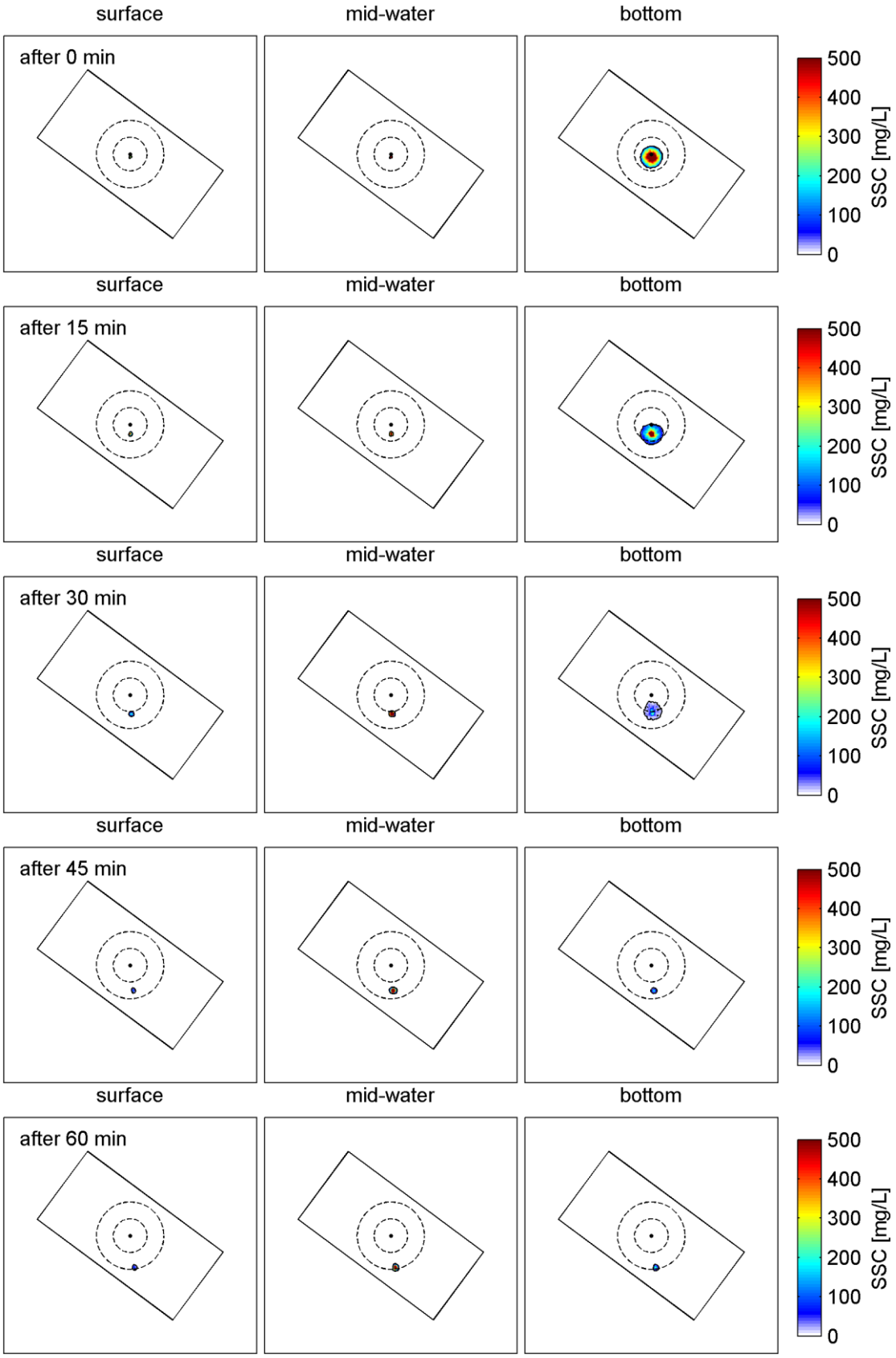

Figure 3.3 Disposal of one load of the Volvox Asia vessel (V=10,800 m^3) at site 5 during strong northeast winds. Dashed circles have radiuses of 500 and 1000 m.

Calm conditions

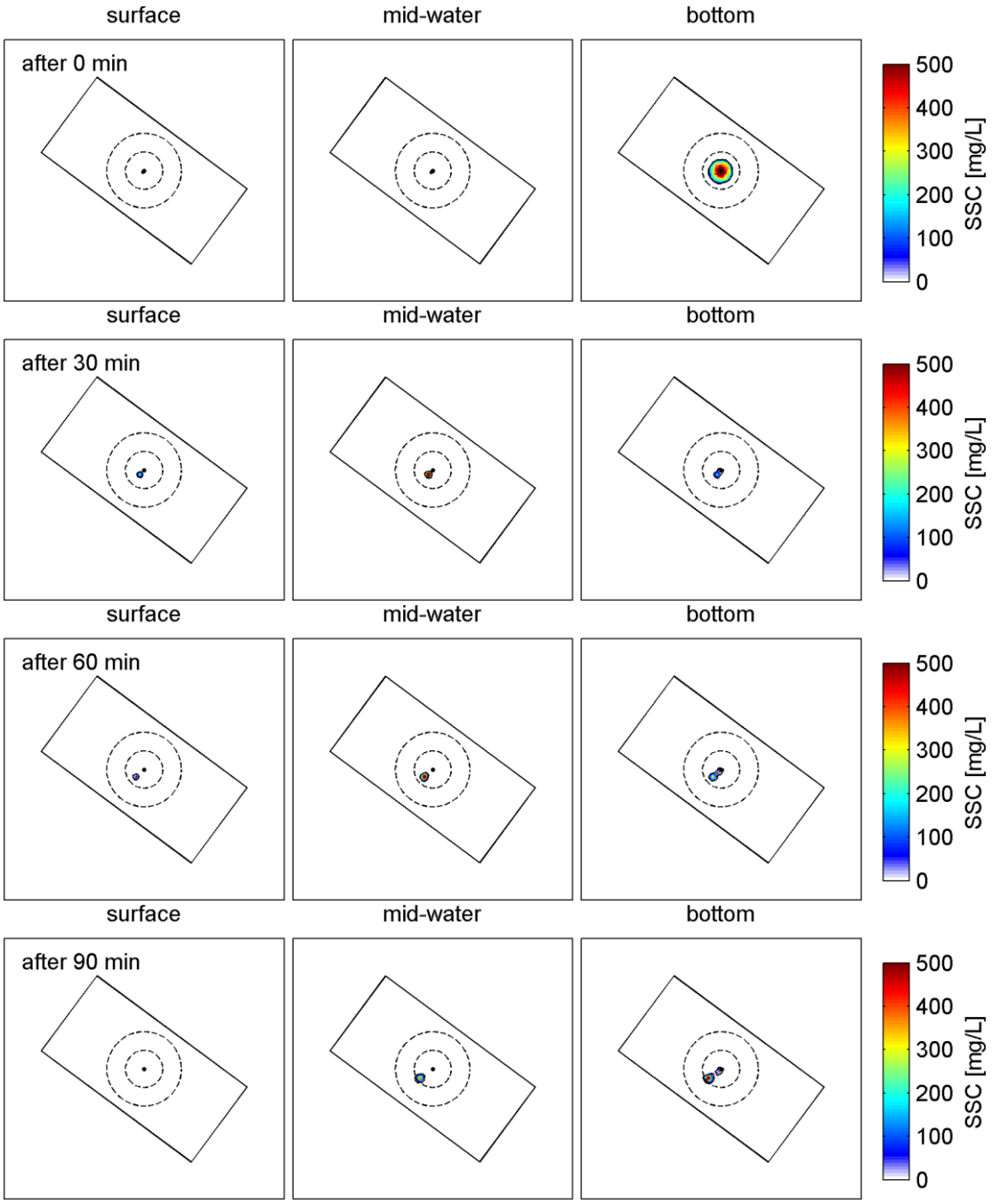

Figure 3.4 Disposal of three successive hopper loads of the Volvox Asia vessel (V=10,800 m^3) at site 5 during calm conditions : time period from 0 to 90 minutes after first disposal. Dashed circles have radiuses of 500 and 1000 m.

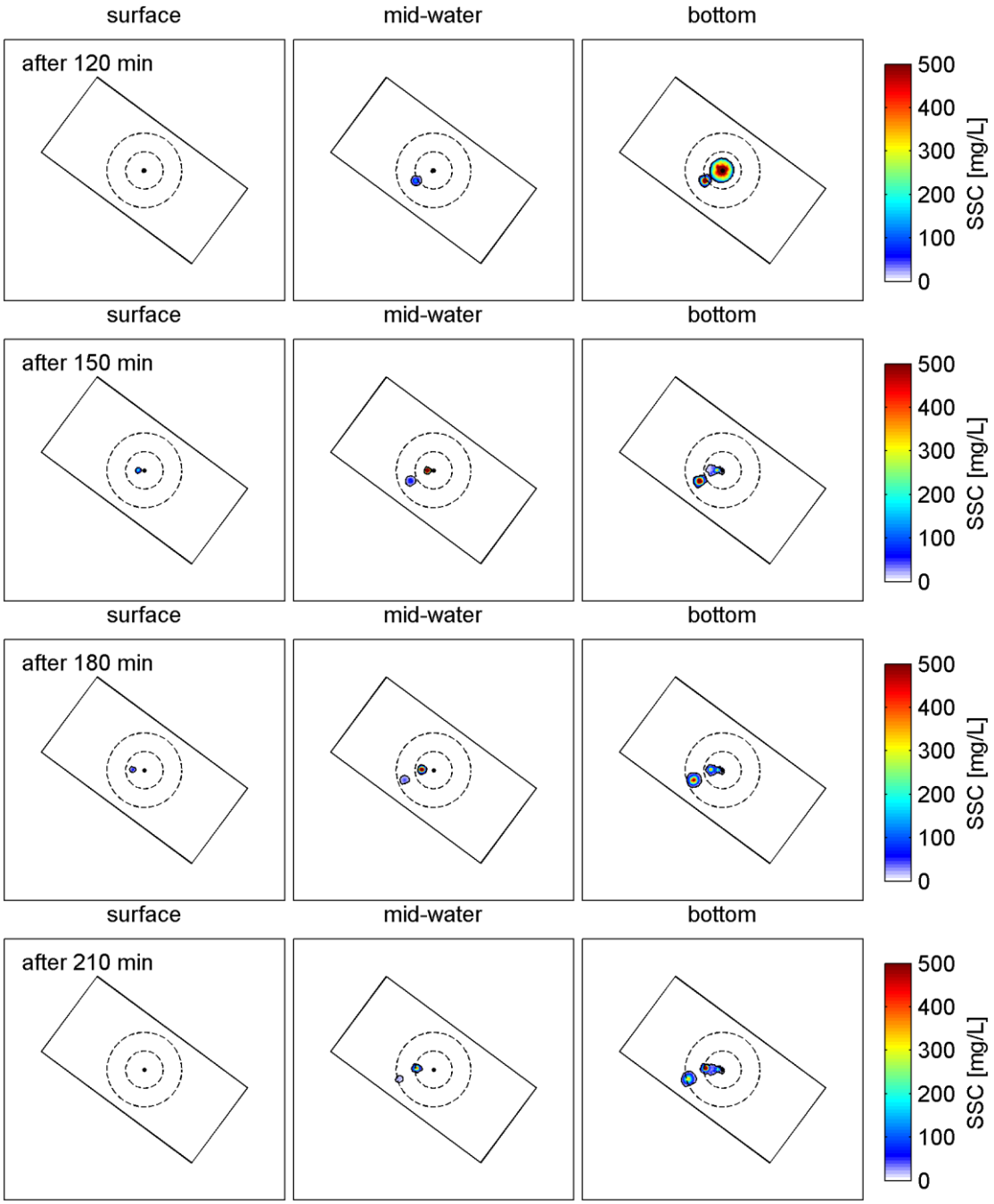

Figure 3.5 Disposal of three successive hopper loads of the Volvox Asia vessel (V=10,800 m^3) at site 5 during calm conditions : time period from 120 to 210 minutes after first disposal. Dashed circles have radiuses of 500 and 1000 m.

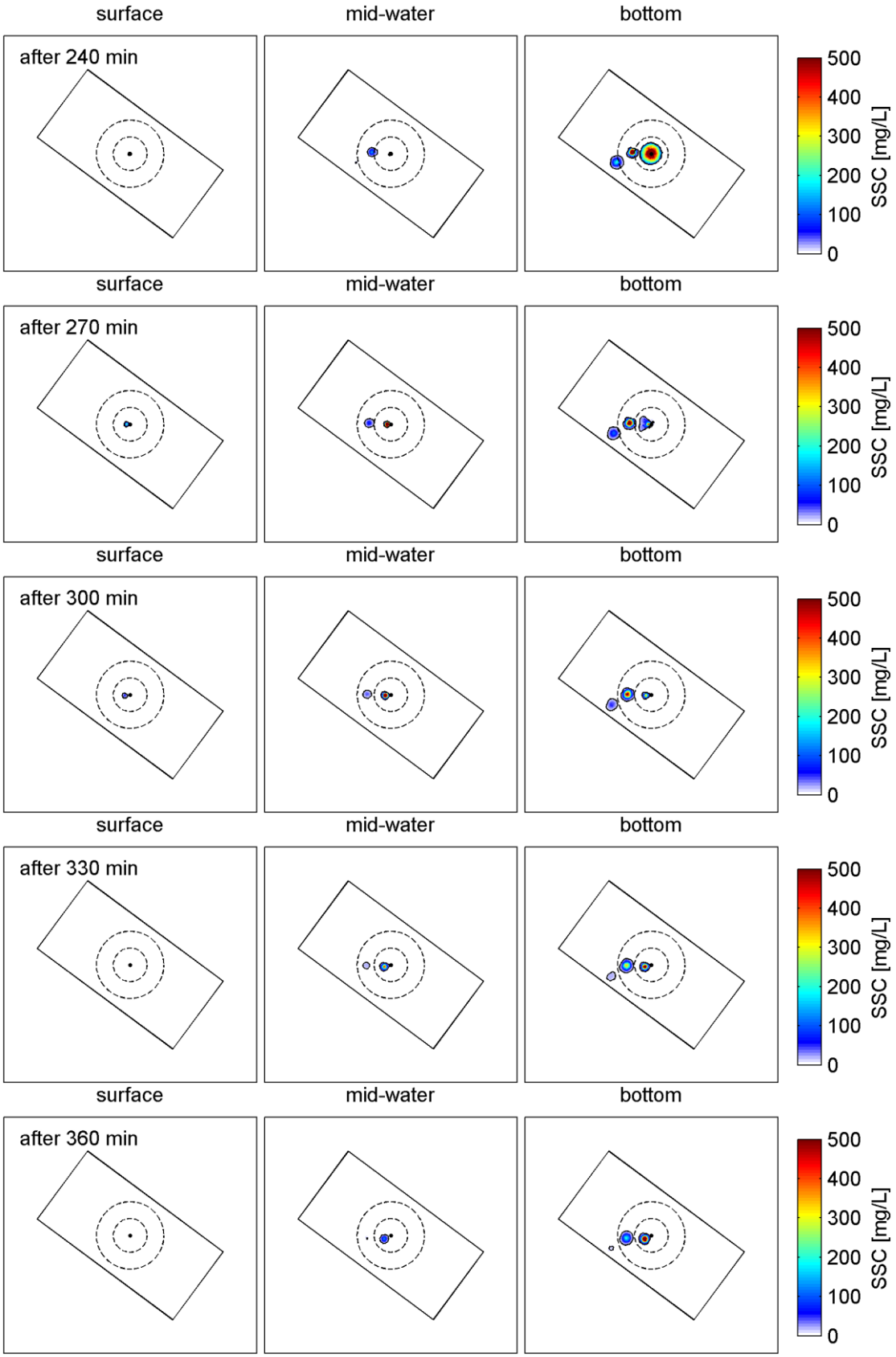

Figure 3.6 Disposal of three successive hopper loads of the Volvox Asia vessel (V=10,800 m^3) at site 5 during calm conditions : time period from 240 to 360 minutes after first disposal. Dashed circles have radiuses of 500 and 1000 m.

3.2. Long-term mean disposal *SSC* plumes and deposition thicknesses derived from the 10 year hindcast

3.2.1. Suspended sediment concentration plumes

In practice, the exact timing of the future disposal operations is unknown and it is therefore beneficial to consider the entire range of forcing conditions that could be encountered at the site to have a more robust picture of the potential plume dispersion patterns. In this study, this issue was addressed by running long-term hindcast simulations of continuous disposal during a 10-year period. The approach allows capturing the entire range of forcing conditions at the site and the resulting *SSC* plume tracks. The results of the 10-year simulations were time-averaged to produce the mean *SSC* fields associated with the disposal of one hopper load. The 10-year time period ensure that the produced results are statistically relevant and produced results should be interpreted as probabilistic, statistically based dispersion patterns of the disposal-related *SSC* plume rather than being representative of an individual plume.

The mean *SSC* plumes resulting from sediment disposal at the centre and corners of the proposed disposal ground, with the Volvox Asia vessel, are presented in Figure 3.7 at a smaller scale to illustrate their positions and extents relative to the shoreline. A larger scaled map of the same set of results is included in Figure 3.8 to better illustrate the local plume patterns. Note the colour scale was adjusted from the figures in Section 3.1 for a better resolution of the smaller *SSC* levels at some distance from the release point.

The *SSC* plumes expectedly show the largest extents and magnitudes in the bottom layer. Relatively high *SSC* levels are found within the 300 metre radius around the release due to the density current source term included in simulations; the overall shape is elliptic in the northwest-southeast axis which is consistent with the tidal ellipse at the site as well as general residual current axis (see Figure 3.8 and report Metocean Solutions Limited P0201-04, 2015). The elliptic shape is reproduced in the mid water layer although with reduced *SSC* plumes extents and concentrations magnitudes. The 10 $mg.L^{-1}$ contour generally stays within 1 km of the disposal location in the bottom layer and within 500 metres in the mid-water layer. In the surface plume, although some *SSC* traces are indeed predicted, extents are very limited and magnitudes remain below 10 $mg.L^{-1}$ (therefore not rendered in the plots).

To provide some sensitivity testing of the source term assumptions, mean *SSC* plumes assuming that 1% and 5% of the total load is de-entrained from the descending density jet of sediment are compared in Figure 3.10. Differences are the most significant in the mid-water layer with the *SSC* plumes logically reducing when the percentage is reduced. In order to maintain a degree of conservatism, but remain within realistic bounds (based on available literature and Spearman, pers. comm.), a 5% de-entrained value is considered most applicable.

Previous results represent the characteristics of the *SSC* plume dispersion assuming the use of the Volvox Asia vessel, which has the intermediate hopper load capacity (i.e. Volvox Asia V=10,800 m^3; Olympia V=5,000 m^3; Utrecht V=18,000 m^3). Mean *SSC* plumes patterns and magnitudes will

effectively be modulated by the choice of the disposal vessels used due to hopper load capacity and thus net amount of sediment released in the water column, but also by the draught depth. Here, the use of the Olympia vessel will result in relatively less sediment released in the water column, but the shallower draught means that a fraction of the sediment will be released higher in the water column and will have more time to disperse from the disposal location. Conversely, more sediment will be released in the water column when using the Utrecht vessel but at a deeper depth which relatively reduces the time for a fraction of the suspended sediment to disperse (see Table 2.3 for vessel details). These modulations are illustrated in Figure 3.11.

Results are interpreted with respect to the Volvox Asia vessel that is used as the base case. *SSC* levels are slightly larger in the mid-water level for the Olympia due to the shallower release but overall magnitudes are reduced, notably in the bottom layer. For the Utrecht vessel, *SSC* plume extents and magnitudes are increased relative to the Volvox Asia vessel. That being, the 10 $mg.L^{-1}$ contour stays within 1 km of the release location in the bottom layer and within 500 metres in the mid-water layer as for the Volvox Asia vessel results. Note a slight southeast skewness is present in the bottom layer plumes (most easily seen for the Utrecht vessel due the larger *SSC* levels), which is consistent with the net flow residual at the site. (see Metocean Solutions Limited P0201-04, 2015; Soutelino and Beamsley 2015).

3.2.1. Depositional footprints

Besides the *SSC* plumes, the 10-year simulations also allow characterizing the expected patterns of sediment deposition associated the passive plume dispersion. The mean sediment deposition fields resulting from the disposal of one hopper load of the Volvox Asia vessel are shown in Figure 3.12. Most of the deposition is distributed within the 300 m radius around the release site with an elliptic shape developing further away from the release site consistent with the *SSC* plume patterns. The 1 mm depositional contour is consistently contained within the 500 m radius around the release location. It is stressed that the presented depositions fields are for the passive plume only and do not include the large fraction that settles immediately to the bottom following the dynamic collapse (~70 %, see Figure 2.6). This fraction of sediment will be contained within the 300 m radius around release position as predicted by the nearfield modelling (Spearman, pers. comm.), with most of the sediment actually depositing in the close vicinity of the point of impact.

A sensitivity test on the amount of sediment de-entrained during the sediment convective descent, similar to what was done for the *SSC* plumes (Figure 3.10), is included in Figure 3.13. The modulation of the depositional thickness for the three considered vessels with different hopper capacities is illustrated in Figure 3.14. Note the deposition thicknesses associated with the larger Utrecht vessel are expectedly larger than for the Volvox Asia vessel, however most of the significant increases are contained within a 300 m radius around the release point and the 1 mm contour remains within 500 m of the disposal location.

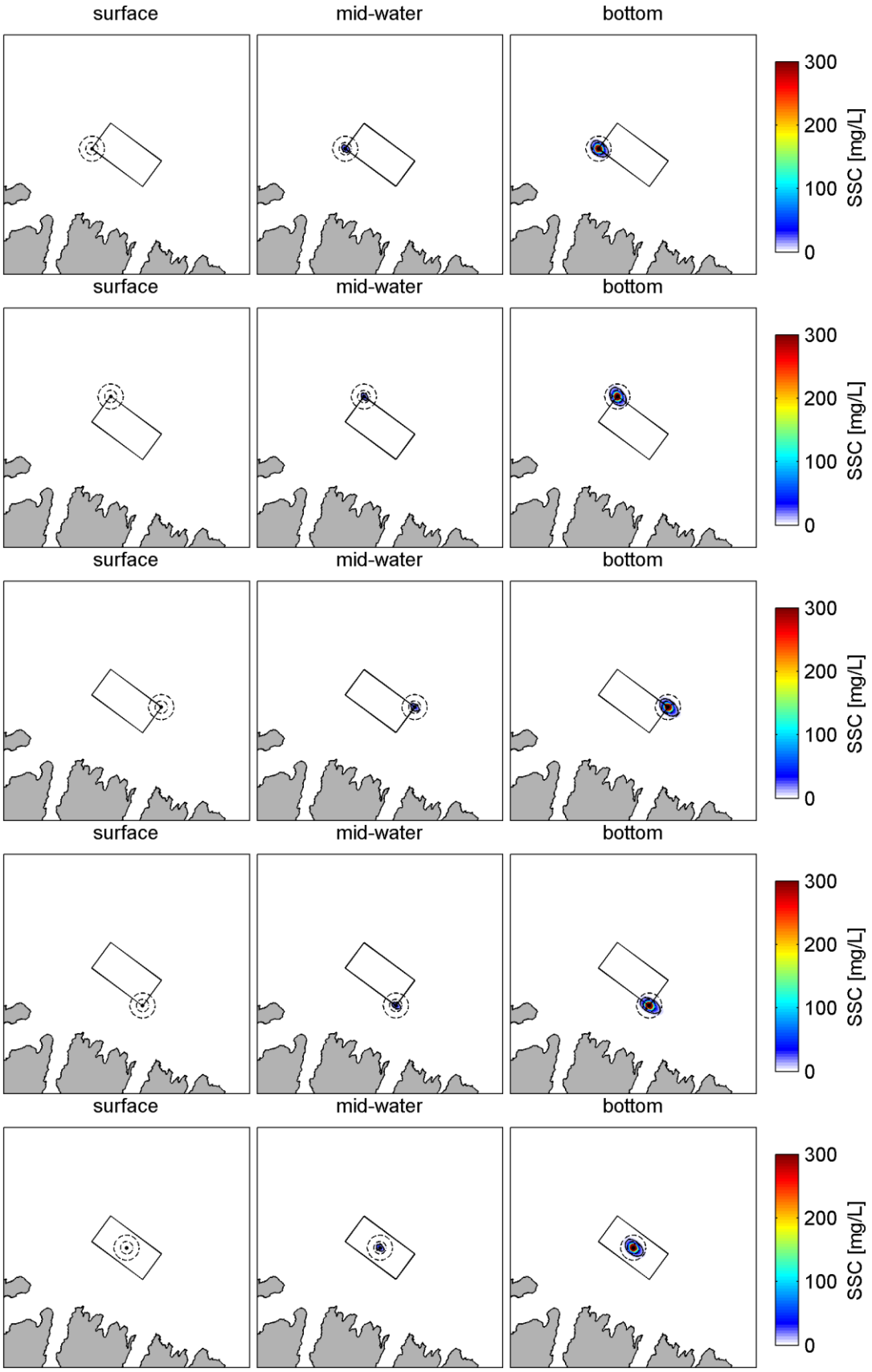

Figure 3.7 Mean *SSC* fields resulting from the disposal of one hopper load of the Volvox Asia vessel (V=10,800 m^3), derived from the 10 year hindcast simulations. The 10 $mg.L^{-1}$ *SSC* contour line is shown in dark. Dashed circles have radiuses of 500 and 1000 m.

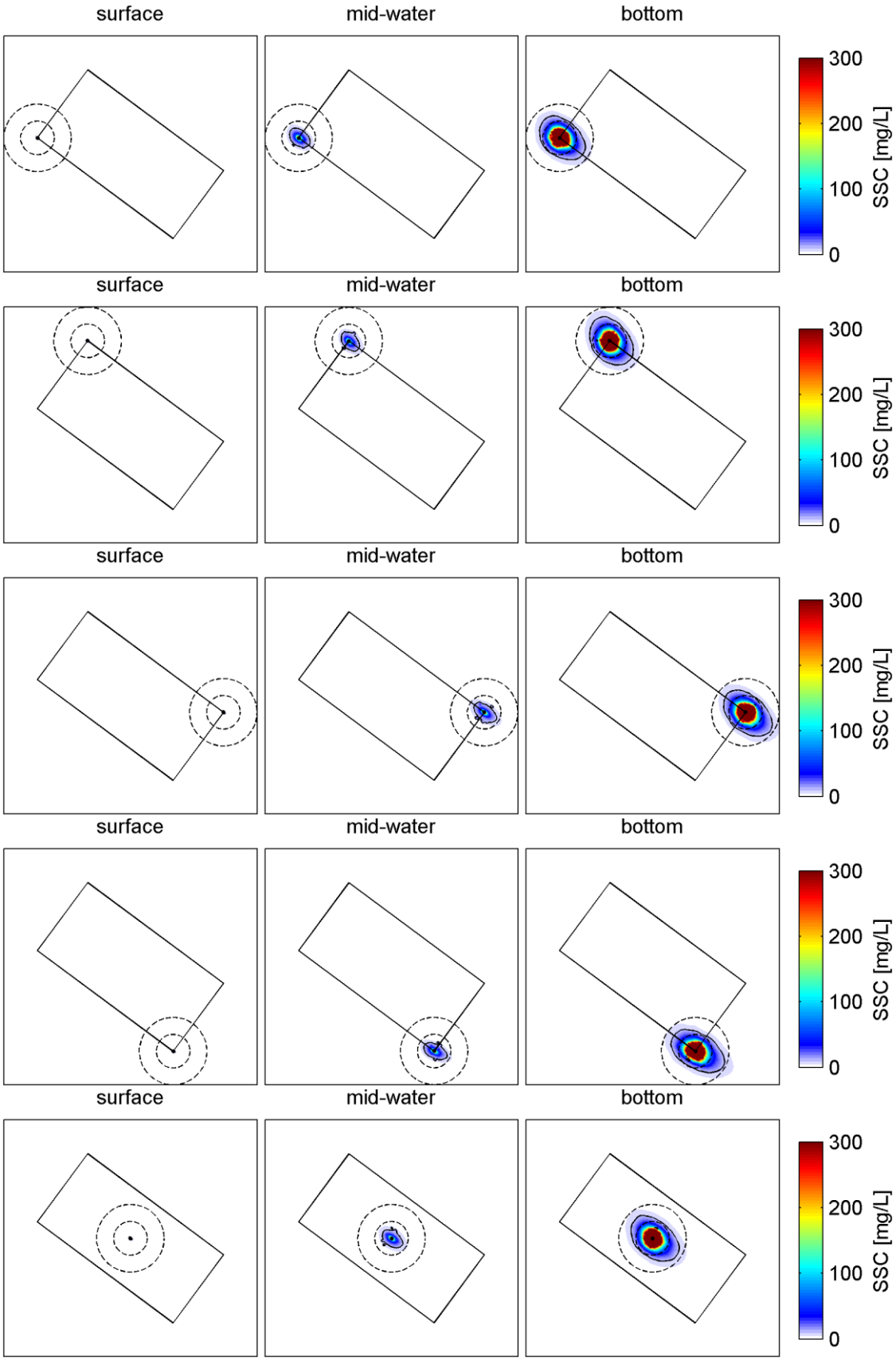

Figure 3.8 Zoomed in view of mean *SSC* fields resulting from the disposal of one hopper load of the Volvox Asia vessel (V=10,800 m^3), derived from the 10 year hindcast simulations. The 10 $mg.L^{-1}$ *SSC* contour line is shown in dark. Dashed circles have radiuses of 500 and 1000 m.

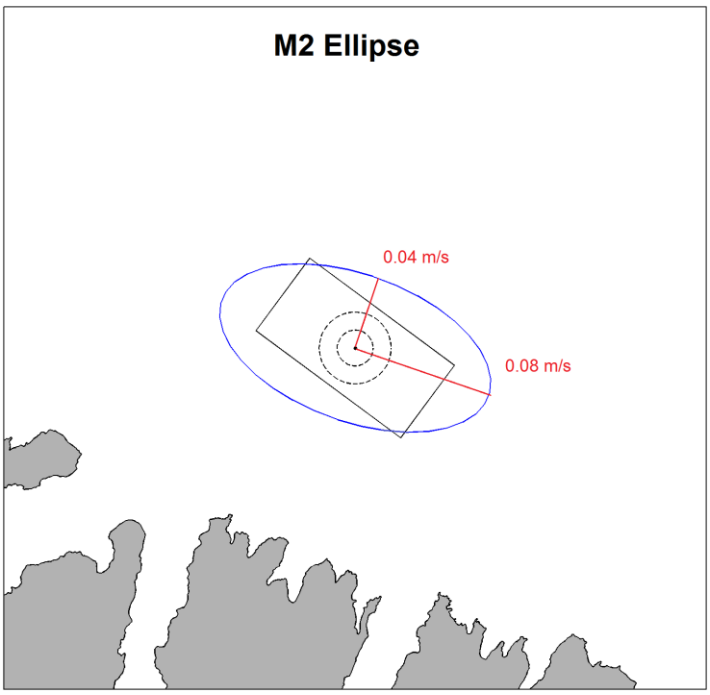

Figure 3.9 M2 tidal constituent ellipse at the site 5 in the centre of the disposal ground.

1 % loss due to sediment stripping during descent

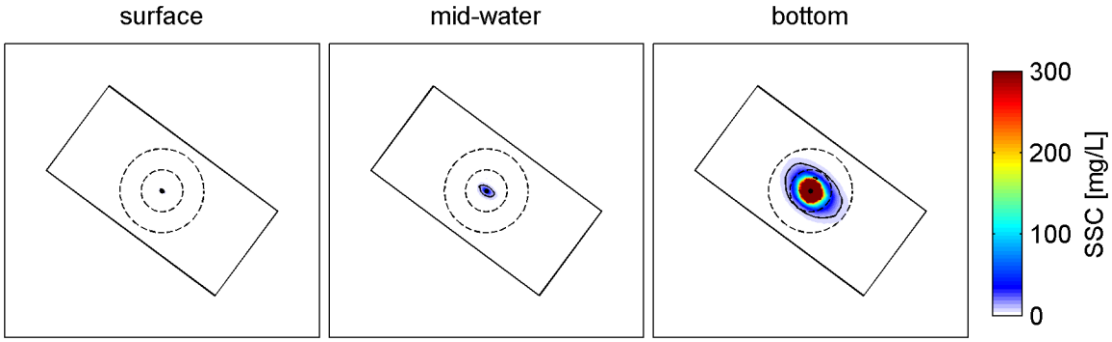

5 % loss due to sediment stripping during descent

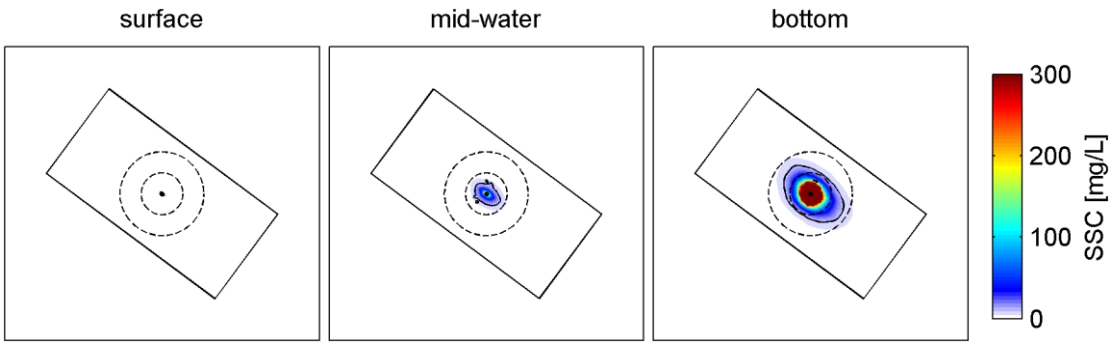

Figure 3.10 Comparison of mean *SSC* fields resulting from the disposal of one hopper load of the Volvox Asia vessel (V=10,800 m^3) at site 5 assuming that 1 % (top) and 5 % (bottom) of the sediment volume is stripped during the convective descent. The 10 $mg.L^{-1}$ *SSC* contour line is shown in dark. Dashed circles have radiuses of 500 and 1000 m.

Volvox Asia (V= 10,800 m^3)

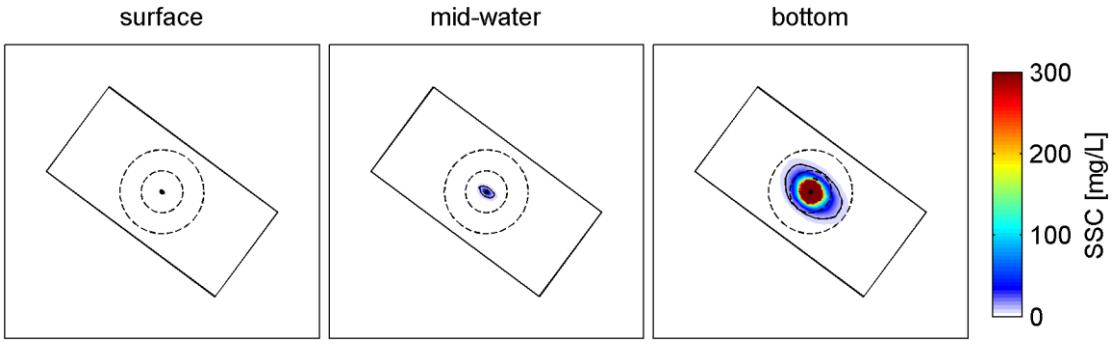

Utrecht (V= 18,000 m^3)

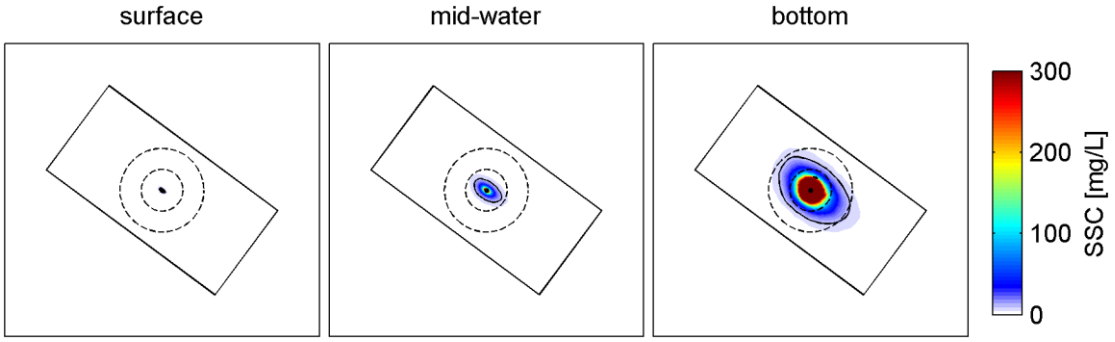

Olympia (V= 5,000 m^3)

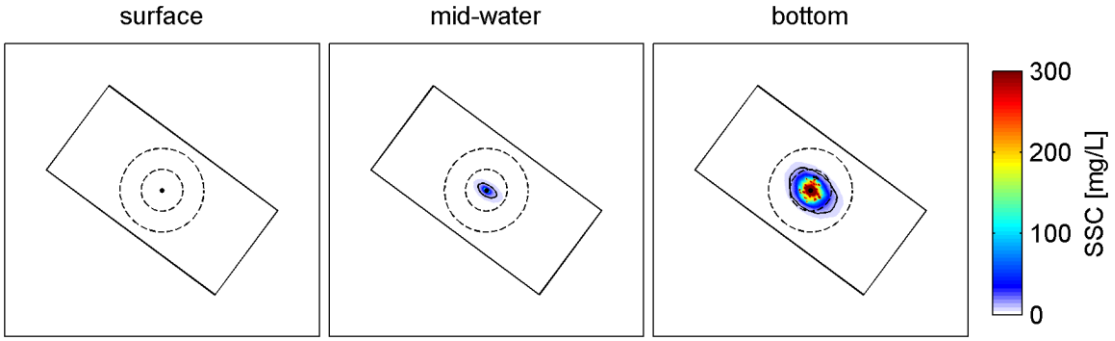

Figure 3.11 Comparison of mean *SSC* fields resulting from the disposal of one hopper load at site 5 for the vessels Volvox Asia, Utrecht, and Olympia (V=10,800, 18,000, and 5,000 m^3, respectively). The 10 mg.L^{-1} *SSC* contour line is shown in dark. Dashed circles have radiuses of 500 and 1000 m.

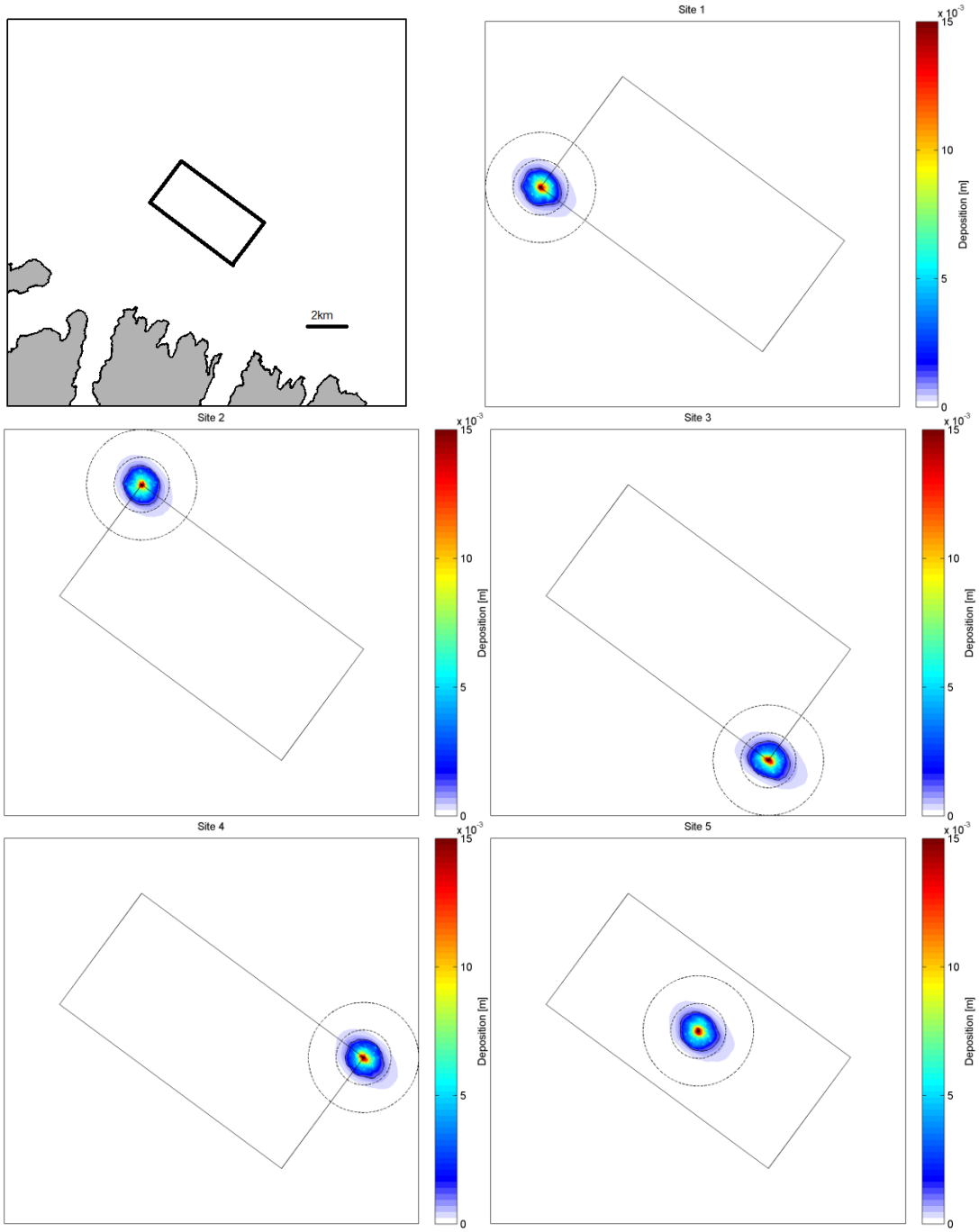

Figure 3.12 Zoomed in view of mean deposition fields resulting from the disposal of one hopper load of the Volvox Asia vessel (V=10,800 m^3), derived from the 10-year hindcast simulations. The 1 mm contour line is shown in dark. Dashed circles have radiuses of 500 and 1000 m.

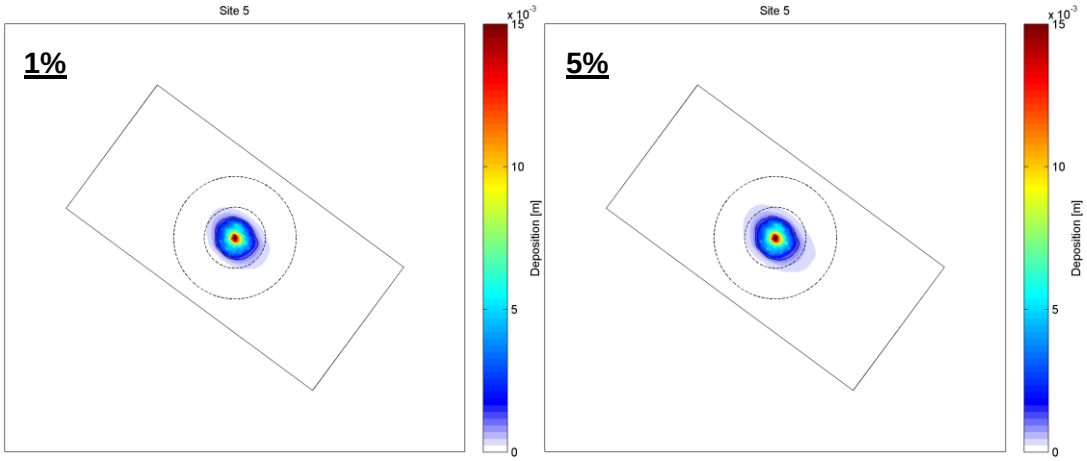

Figure 3.13 Comparison of mean deposition fields resulting from the disposal of one hopper load of the Volvox Asia vessel (V=10,800 m^3) at site 5 assuming that 1 % (left) and 5 % (right) of the sediment volume is stripped during the convective descent. The 1 mm contour line is shown in dark. Dashed circles have radiuses of 500 and 1000 m.

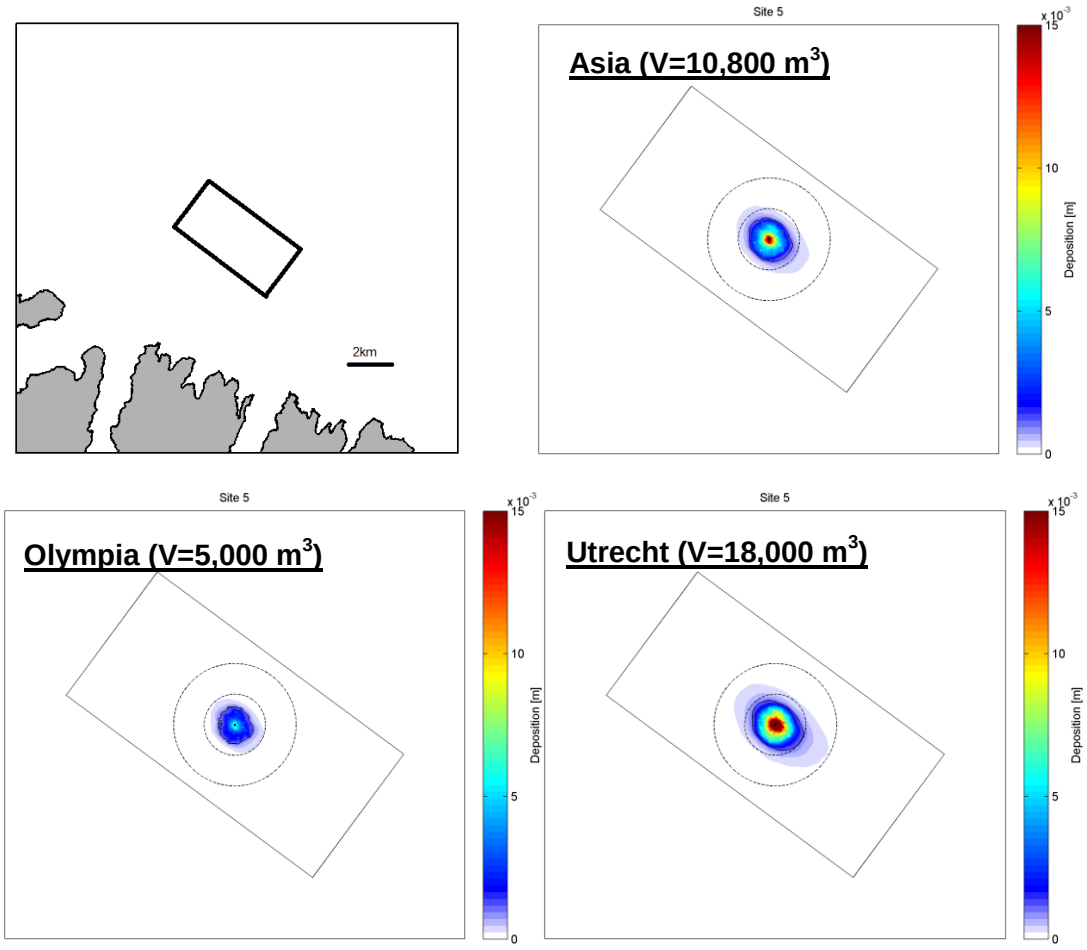

Figure 3.14 Comparison of mean deposition fields resulting from the disposal of one hopper load at site 5 for the vessels Volvox Asia, Utrecht, and Olympia (V_{load}=10,800, 18,000, and 5,000 m^3, respectively). The 1 mm contour line is shown in dark. Dashed circles have radiuses of 500 and 1000 m.

3.3. *SSC* threshold exceedance during disposal activities

Besides the general patterns of the disposal plume dispersion and deposition, an important metric of the disposal-related plumes is the percentage of time a given *SSC* level is exceeded during disposal operations; notably in the context of ecological impact assessment for example.

This section includes such exceedance time percentage for three *SSC* thresholds, i.e. 10, 50 and 100 $mg.L^{-1}$. These thresholds were chosen based on the empirical information available on the ambient *SSC* levels within Pegasus Bay (i.e. naturally occurring, see section 2.7). The available records suggest mean levels in the typical range of 10-20 $mg.L^{-1}$, reaching levels of the order 50 $mg.L^{-1}$ at times, while values of up to 100 $mg.L^{-1}$ are assumed to occur in rare occasions given the sediment entering the environs from river and overland run-offs.

The determination of the exceedance time percentage can become very computationally demanding because it requires estimating full concentration fields at every time step of the simulation. In the present application, two–hourly sediment disposals were simulating continuously over a 1-month period spanning both January and August 2010, capturing typical summer and winter forcing conditions, respectively.

Results are presented for disposal at the centre of the disposal ground (site 5), as well as site 3 which is the corner of the disposal ground closest to the shoreline, and assuming disposal with the intermediate vessel size Volvox Asia. These were supplemented by shorter term simulations during the energetic and calm events considered in section 3.1 (see Table 2.6 and Figure 2.7) which can be useful in the context of an adaptive management of the disposal operations with respect to the instantaneous forcing conditions.

The exceedance time percentages are presented in Figure 3.15 and Figure 3.16 for the summer month of January and in Figure 3.17 and Figure 3.18 for the winter month of August. The results generally indicate that near-bed *SSC* thresholds are more frequently sustained or exceeded, and have a greater spatial spread compared with both the mid and near-surface concentrations. These results are consistent with results presented in the previous sections. As expected, the actual extents of the predicted SSC exceedance patches reduces as the SSC threshold increases from 10, to 50 and 100 $mg.L^{-1}$.

For the January simulations, in the near-bed layer the 10 $mg.L^{-1}$ threshold is typically exceeded 10-15 % of the time within a radius of ~300 m of the disposal site. Exceedance times of order 5 % may extend up to ~1 km from the release position and tapper off to zero with distance. In the mid-water level, exceedances of up to 5 % are contained within a 500 m radius and become insignificant past the 1 km radius. The 10 $mg.L^{-1}$ is very rarely exceeded in the surface layers.

The overall exceedance regions reduce as the *SSC* thresholds are increased. However even the 100 $mg.L^{-1}$ level is expected to be exceeded in the near-bed layer for approximately 5-10 % of the time (within 100-200 m radius of the disposal site). This indicates that instantaneous *SSC* levels can be relatively high in the near-bed layer; however associated extents are

relatively limited. It is important to recognise that repeated disposal at the same site introduces a degree of conservatism in these predictions because in practice, sediment disposal will be spread throughout the disposal ground.

No significant differences are visible between the exceedance patterns considering disposal at sites 3 and 5. With respect to potential coastal impacts, site 3 results show that even the low exceedance contours (e.g. <1 % exceedance time) remains 2-3 km from the closest point to the shoreline.

The general magnitudes of the percentages of time each *SSC* threshold level is exceeded in each water column layer are slightly larger in August (Figure 3.17, Figure 3.18) than in January (Figure 3.15, Figure 3.16). This modulation is due to the plumes being typically more elongated along the northwest-southeast axis, resulting in slightly higher probability of *SSC* exceeded thresholds along that main northwest-southeast axis. This contrasts with the relatively more homogenous spreading of the plumes in January (i.e. more circular contours). Note, a slight southeast skewness, consistent with the residual current regime, is again present.

Similar exceedance plots have been produced assuming continuous disposal activities at a single site (i.e. hopper load release every 2-hours) under the forcing events given in Section 3.1 (see Table 2.6 and Figure 2.7). Each simulation was run during a 2-day period centred on the event peak. Because of the shorter simulation duration (2 days, compared with a complete month), the results tend to show a more banded appearance, with individual dredge discharge plumes distinguishable. Results for release at sites 5 and 3 are given in Figure 3.19 to Figure 3.26, and illustrate that consecutive disposals at the same location can increase the frequency of *SSC* exceeding the different thresholds (i.e. up to ~20-25% in the bottom layer). An increased frequency of threshold exceedance is expected for both the energetic and more ambient conditions, due to the sequential plumes being dispersed in a consistent direction (e.g. strong current) and limited potential for dispersion under calm conditions, respectively.

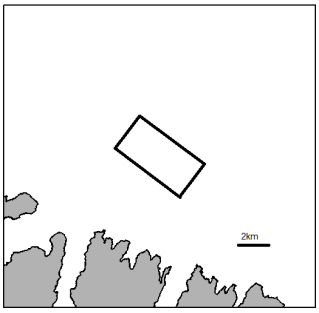

January - Site 5

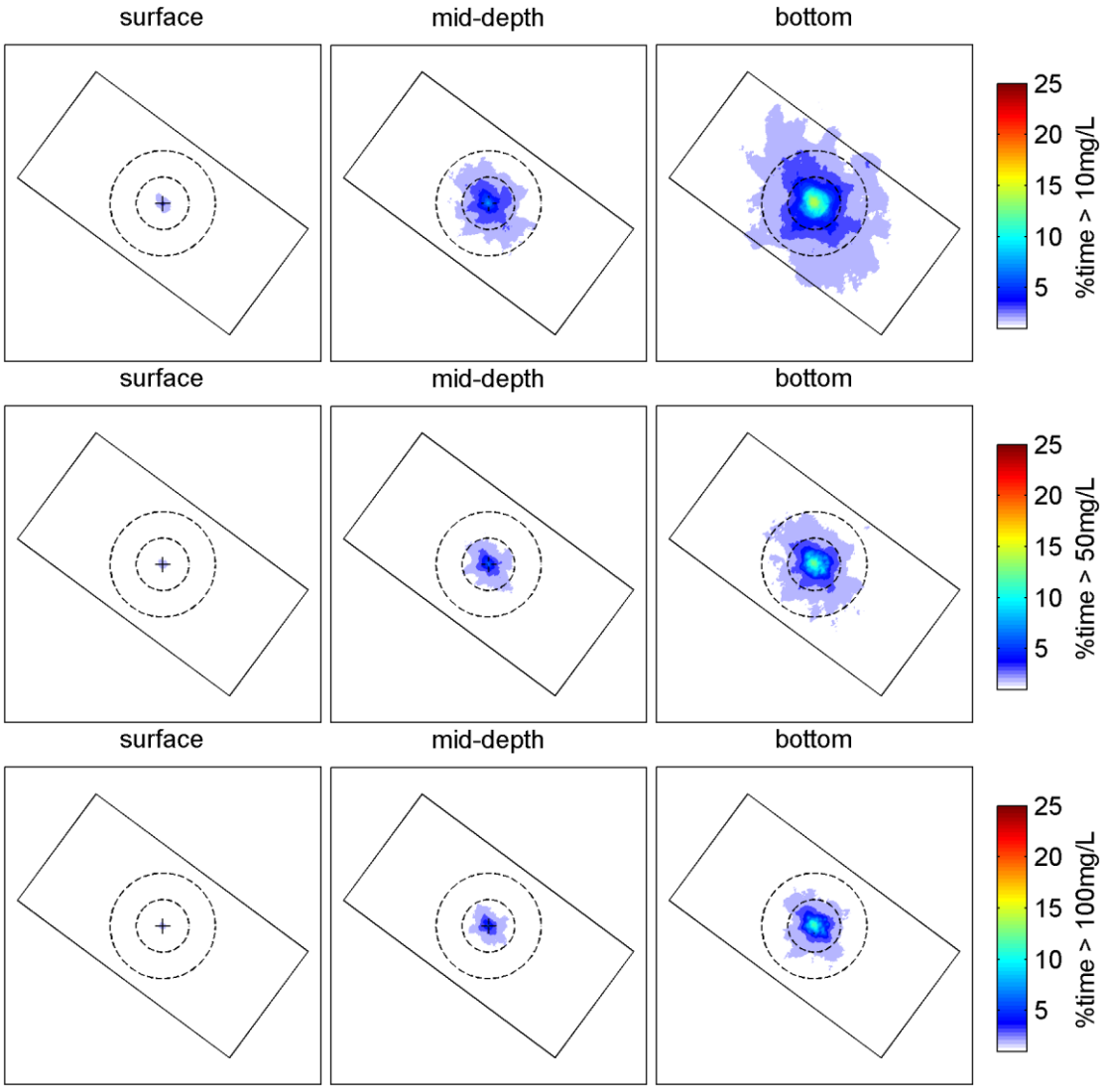

Figure 3.15 Percentage of time *SSC* thresholds of 10, 50, 100 mg.L^{-1} are exceeded during the summer month of January, assuming 2-hourly disposal at site 5 with the Volvox Asia vessel (V=10,800 m^3). Dashed circles have radiuses of 500 and 1000 m. Background concentrations are of the order 10 mg/L

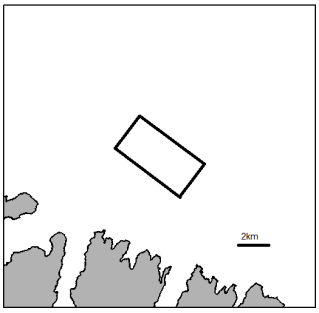

January - Site 3

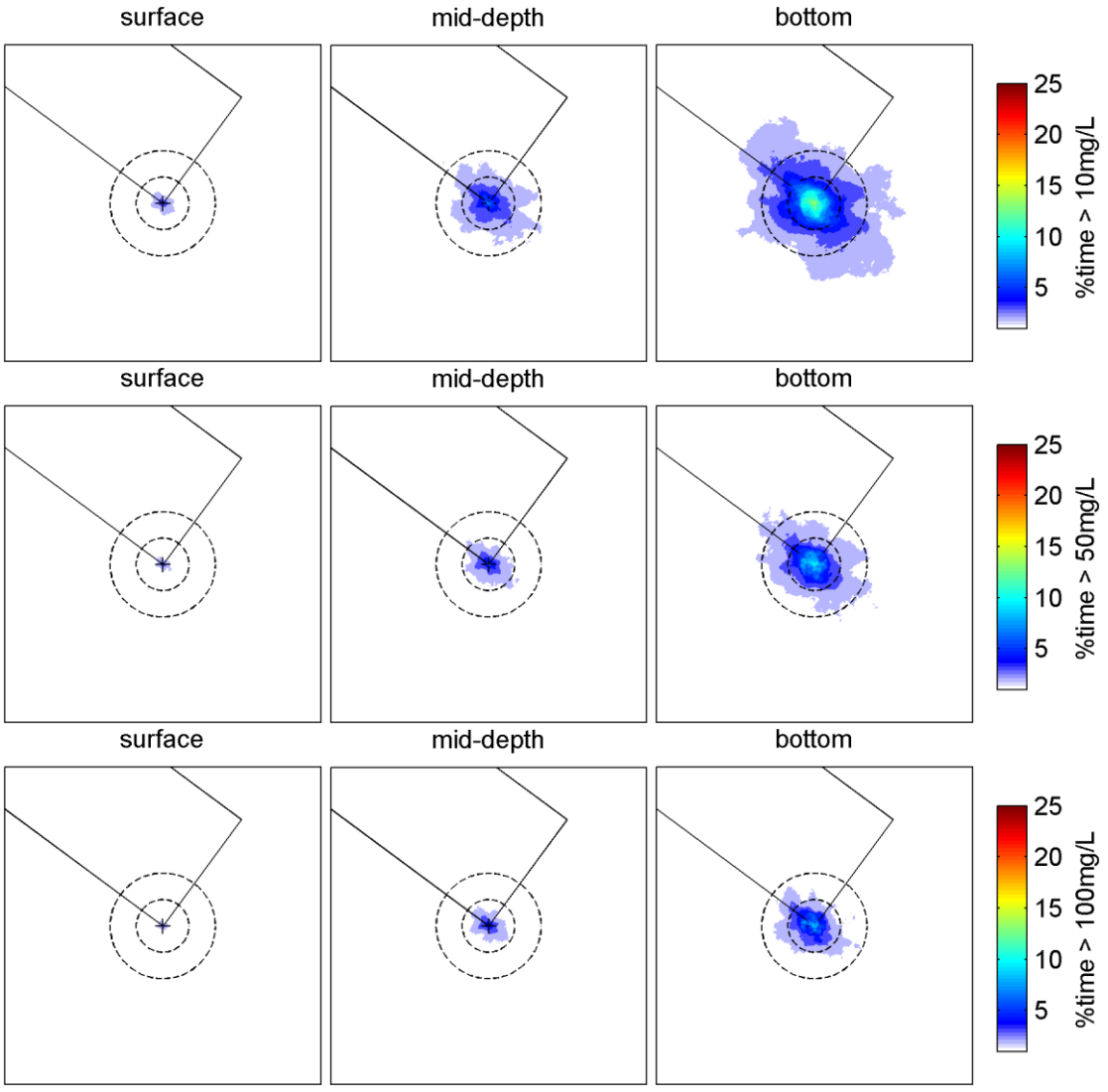

Figure 3.16 Percentage of time *SSC* thresholds of 10, 50, 100 mg.L^{-1} are exceeded during the summer month of January, assuming 2-hourly disposal at site 3 with the Volvox Asia vessel (V=10,800 m^3). Dashed circles have radiuses of 500 and 1000 m. Background concentrations are of the order 10 mg/L

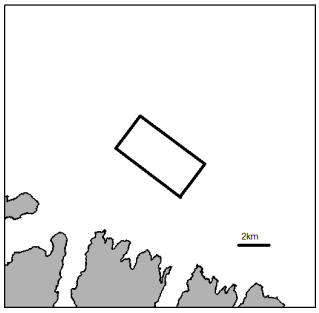

August - Site 5

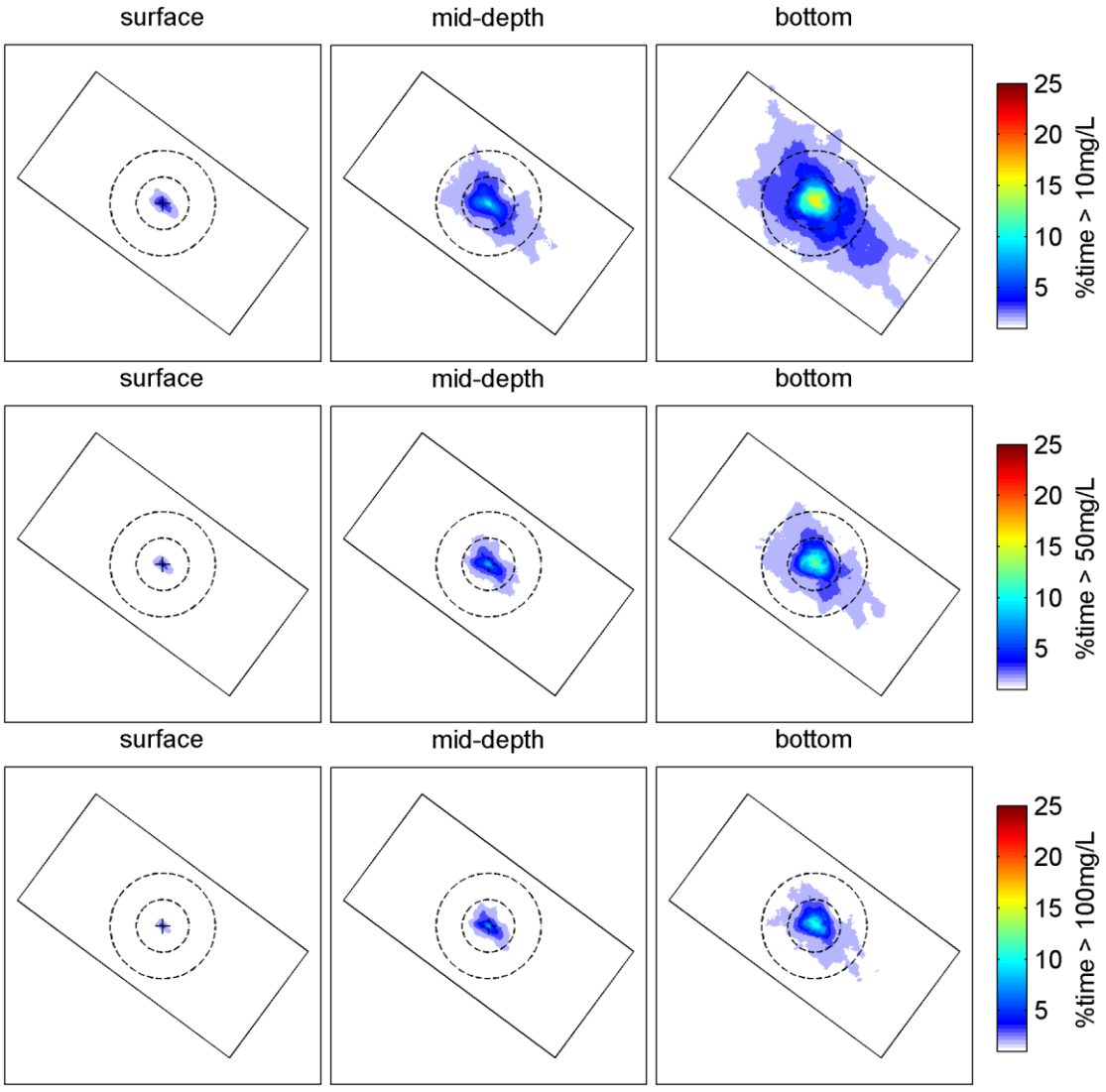

Figure 3.17 Percentage of time *SSC* thresholds of 10, 50, 100 mg.L^{-1} are exceeded during the winter month of August, assuming 2-hourly disposal at site 5 with the Volvox Asia vessel (V=10,800 m^3). Dashed circles have radiuses of 500 and 1000 m. Background concentrations are of the order 10 mg/L

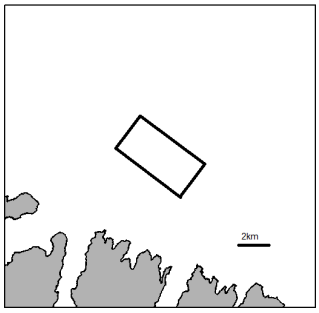

August - Site 3

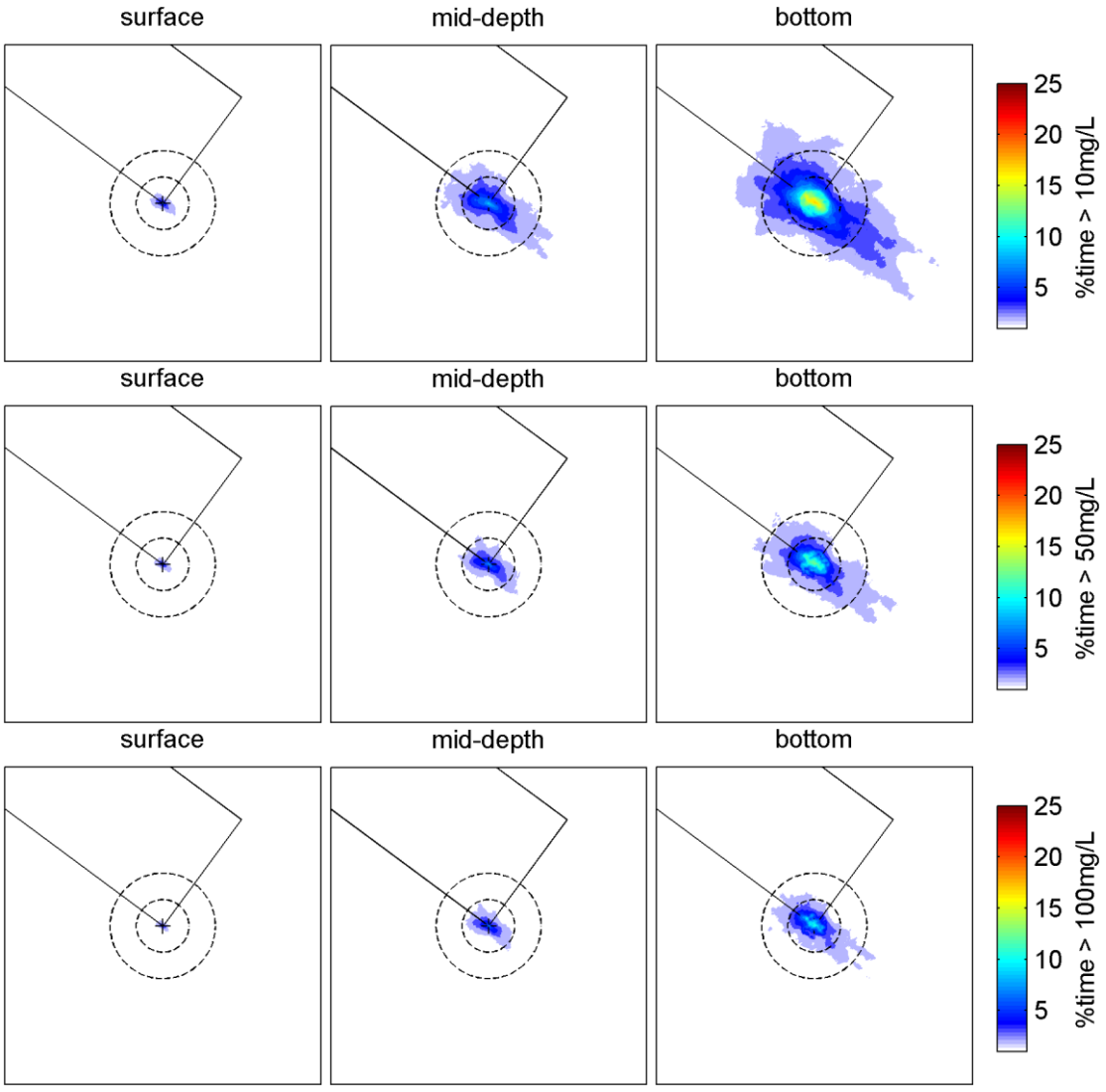

Figure 3.18 Percentage of time *SSC* thresholds of 10, 50, 100 mg.L^{-1} are exceeded during the winter month of August, assuming 2-hourly disposal at site 3 with the Volvox Asia vessel (V=10,800 m^3). Dashed circles have radiuses of 500 and 1000 m. Background concentrations are of the order 10 mg/L

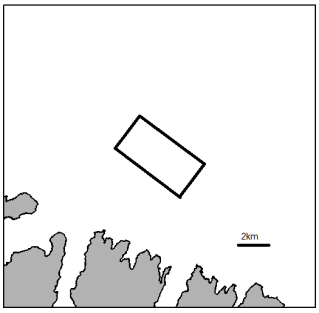

Northwest current

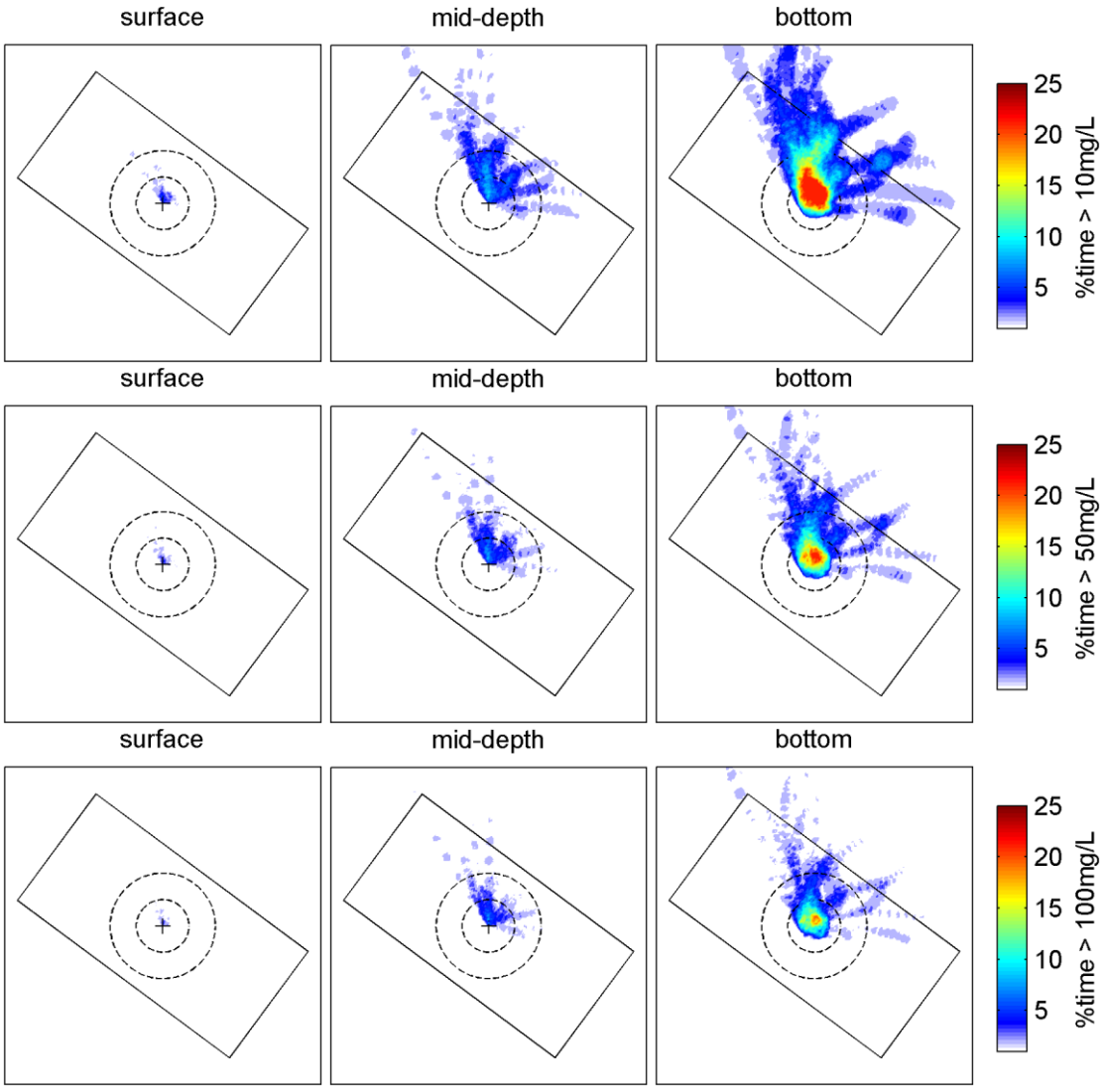

Figure 3.19 Percentage of time *SSC* thresholds of 10, 50, 100 mg.L^{-1} are exceeded during a strong northwest current event, assuming 2-hourly disposal at site 5 with the Volvox Asia vessel (V=10,800 m^3). Dashed circles have radiuses of 500 and 1000 m. Background concentrations are of the order 10 mg/L

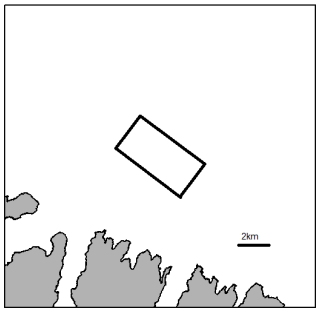

Southeast current

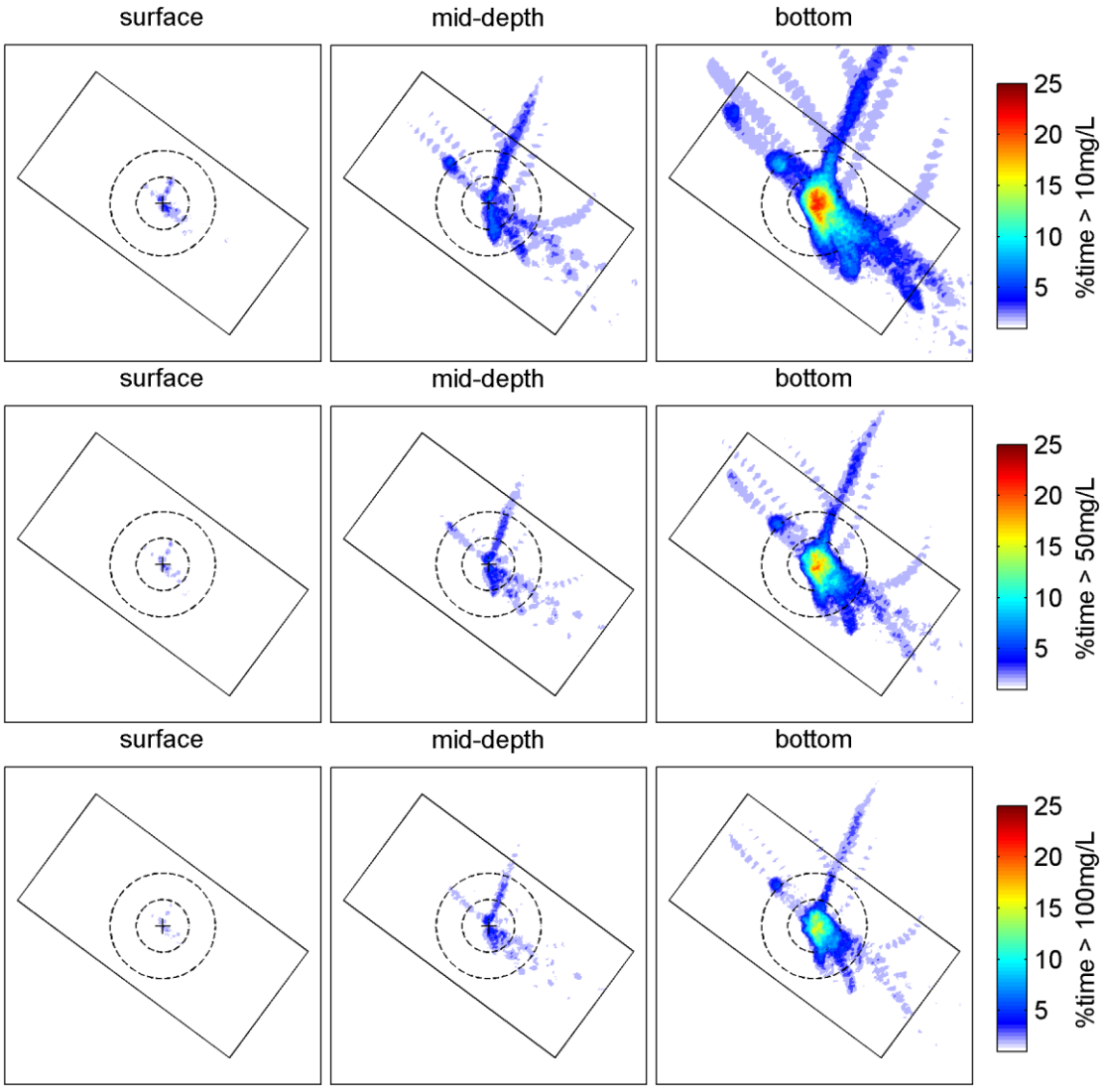

Figure 3.20 Percentage of time *SSC* thresholds of 10, 50, 100 mg.L^{-1} are exceeded during a strong southeast current event, assuming 2-hourly disposal at site 5 with the Volvox Asia vessel (V=10,800 m^3). Dashed circles have radiuses of 500 and 1000 m. Background concentrations are of the order 10 mg/L

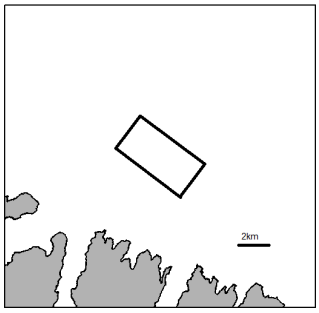

Northeast wind/wave

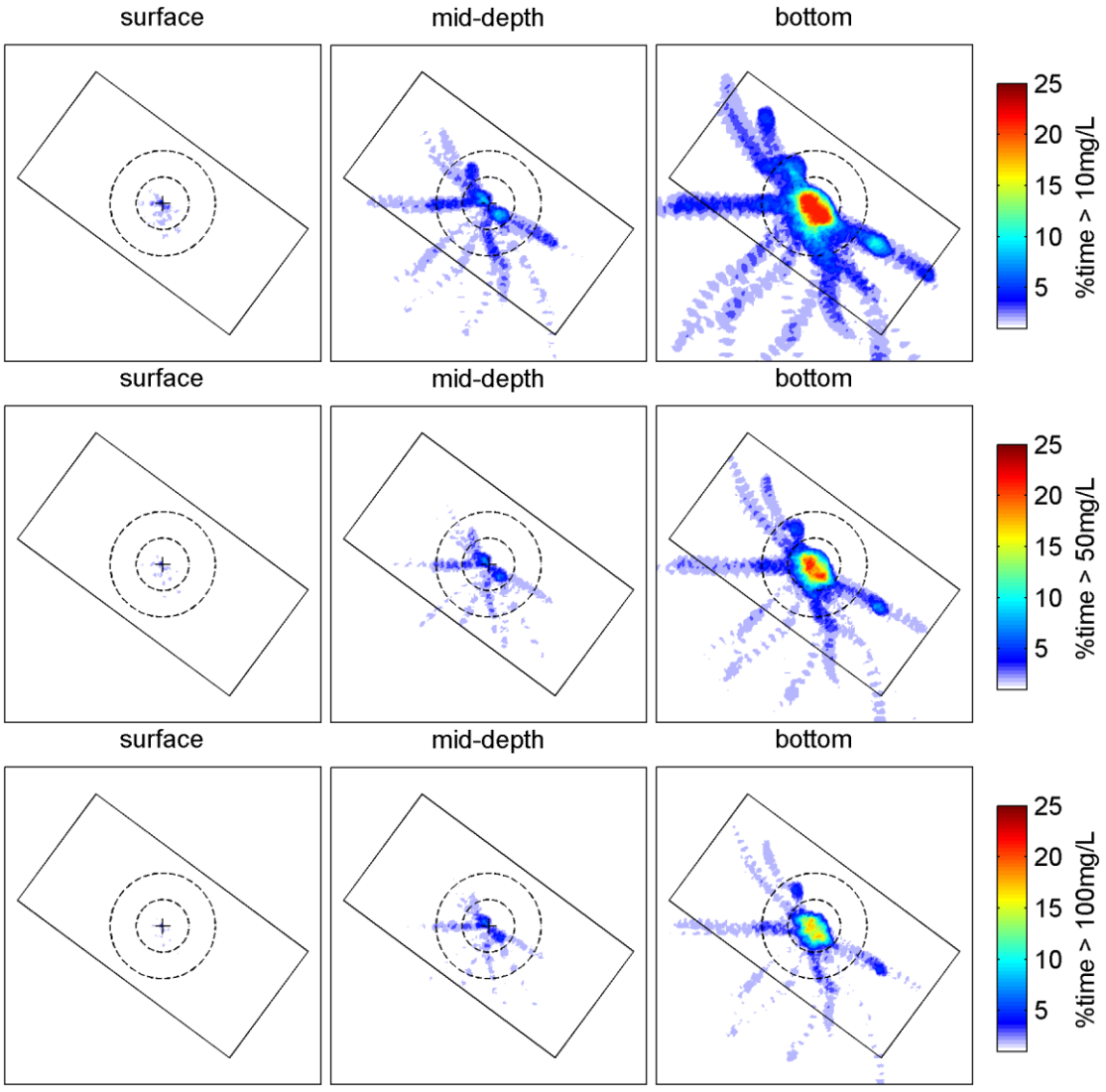

Figure 3.21 Percentage of time *SSC* thresholds of 10, 50, 100 mg.L^{-1} are exceeded during a strong northeast wind/wave event, assuming 2-hourly disposal at site 5 with the Volvox Asia vessel (V=10,800 m^3). Dashed circles have radiuses of 500 and 1000 m. Background concentrations are of the order 10 mg/L

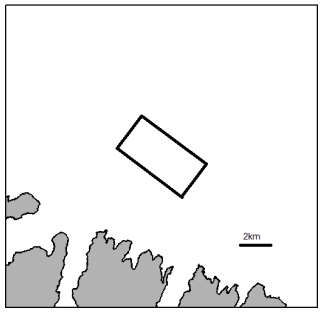

Calm conditions

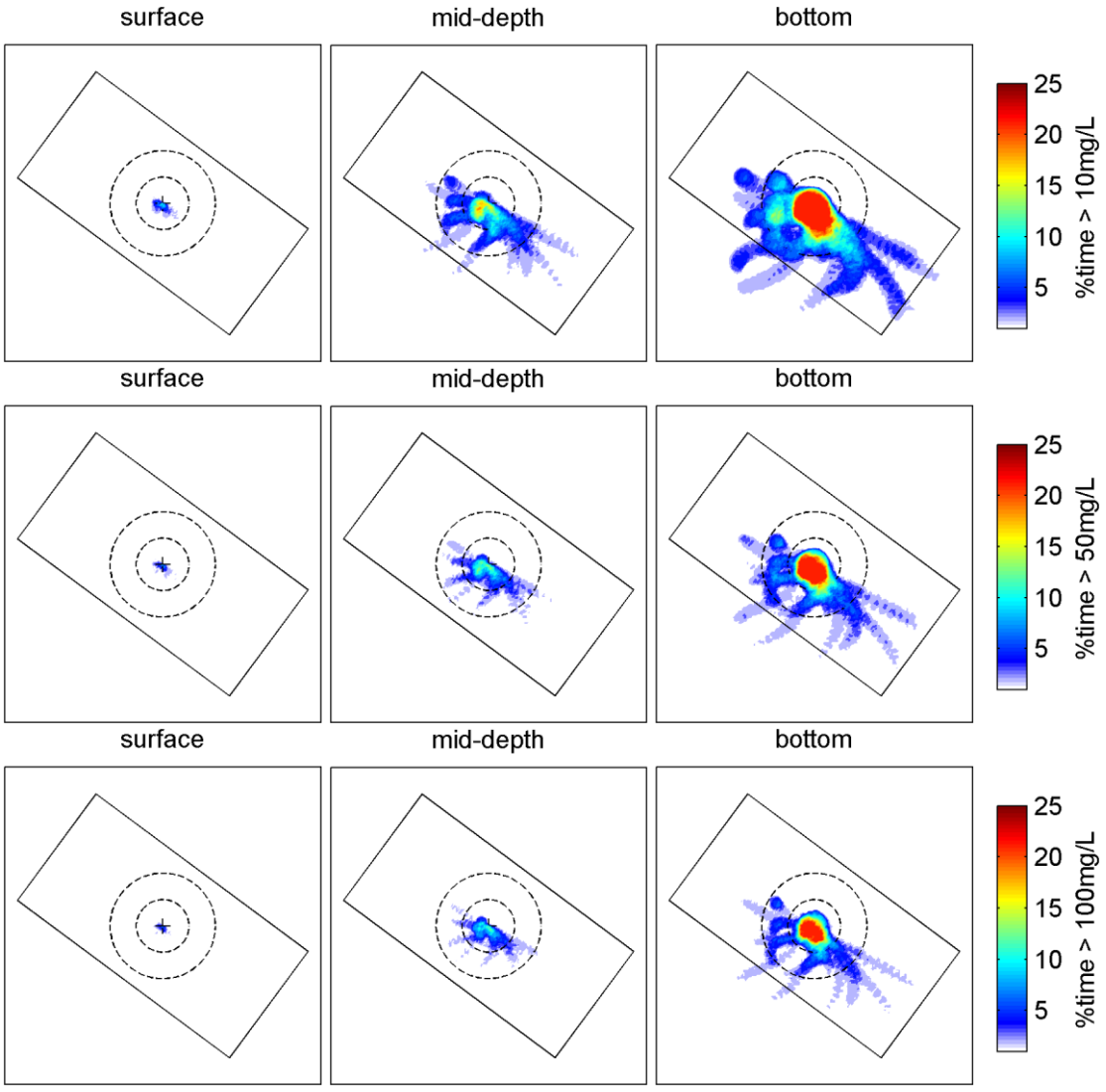

Figure 3.22 Percentage of time *SSC* thresholds of 10, 50, 100 mg.L^{-1} are exceeded during calm conditions assuming, 2-hourly disposal at site 5 with the Volvox Asia vessel (V=10,800 m^3). Dashed circles have radiuses of 500 and 1000 m. Background concentrations are of the order 10 mg/L

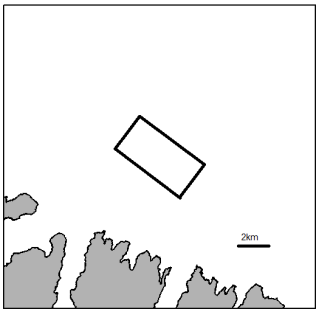

Northwest current

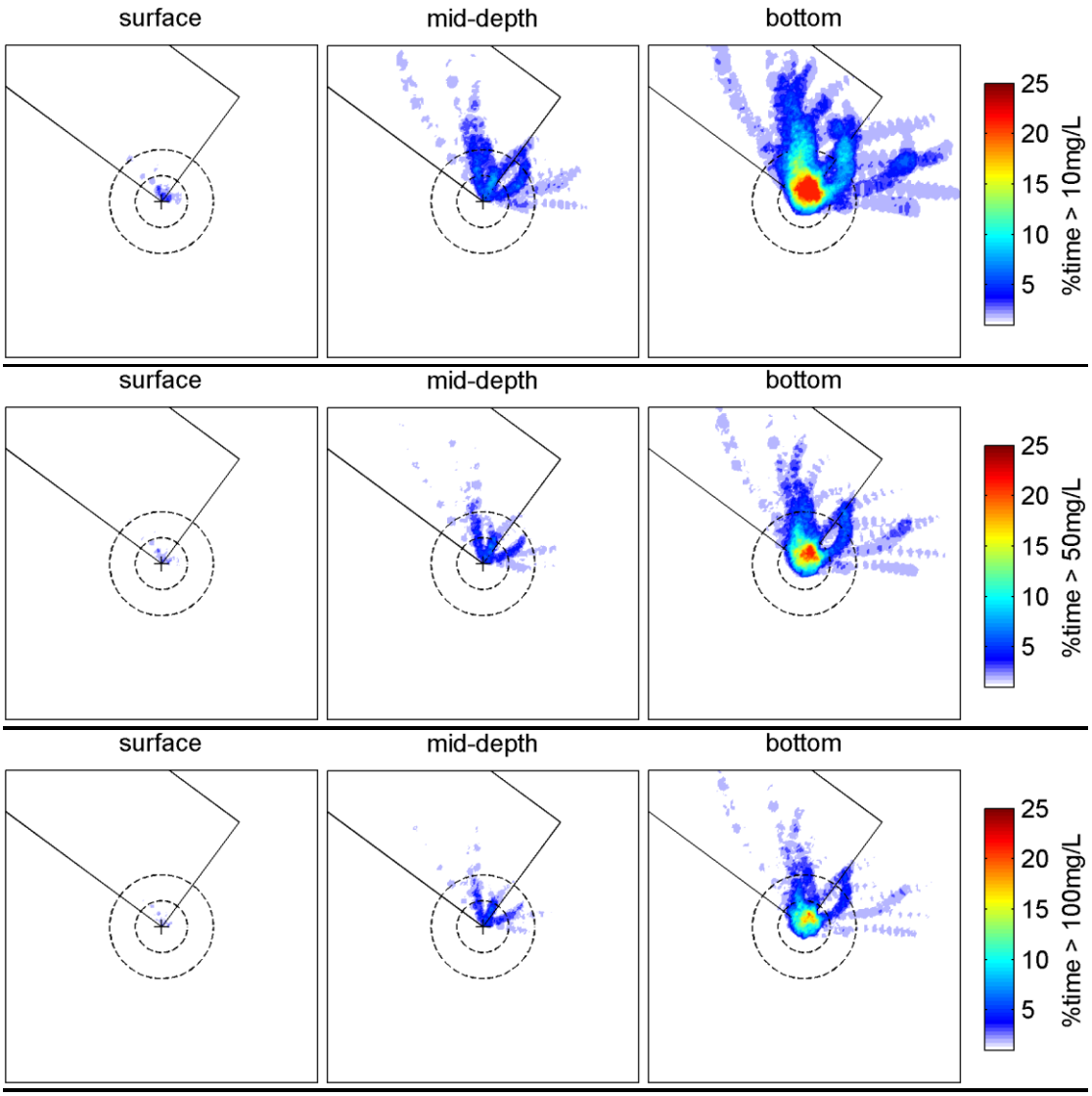

Figure 3.23 Percentage of time *SSC* thresholds of 10, 50, 100 mg.L^{-1} are exceeded during a strong northwest current event, assuming 2-hourly disposal at site 3 with the Volvox Asia vessel (V=10,800 m^3). Dashed circles have radiuses of 500 and 1000 m. Background concentrations are of the order 10 mg/L

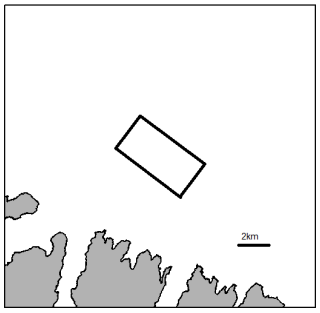

Southeast current

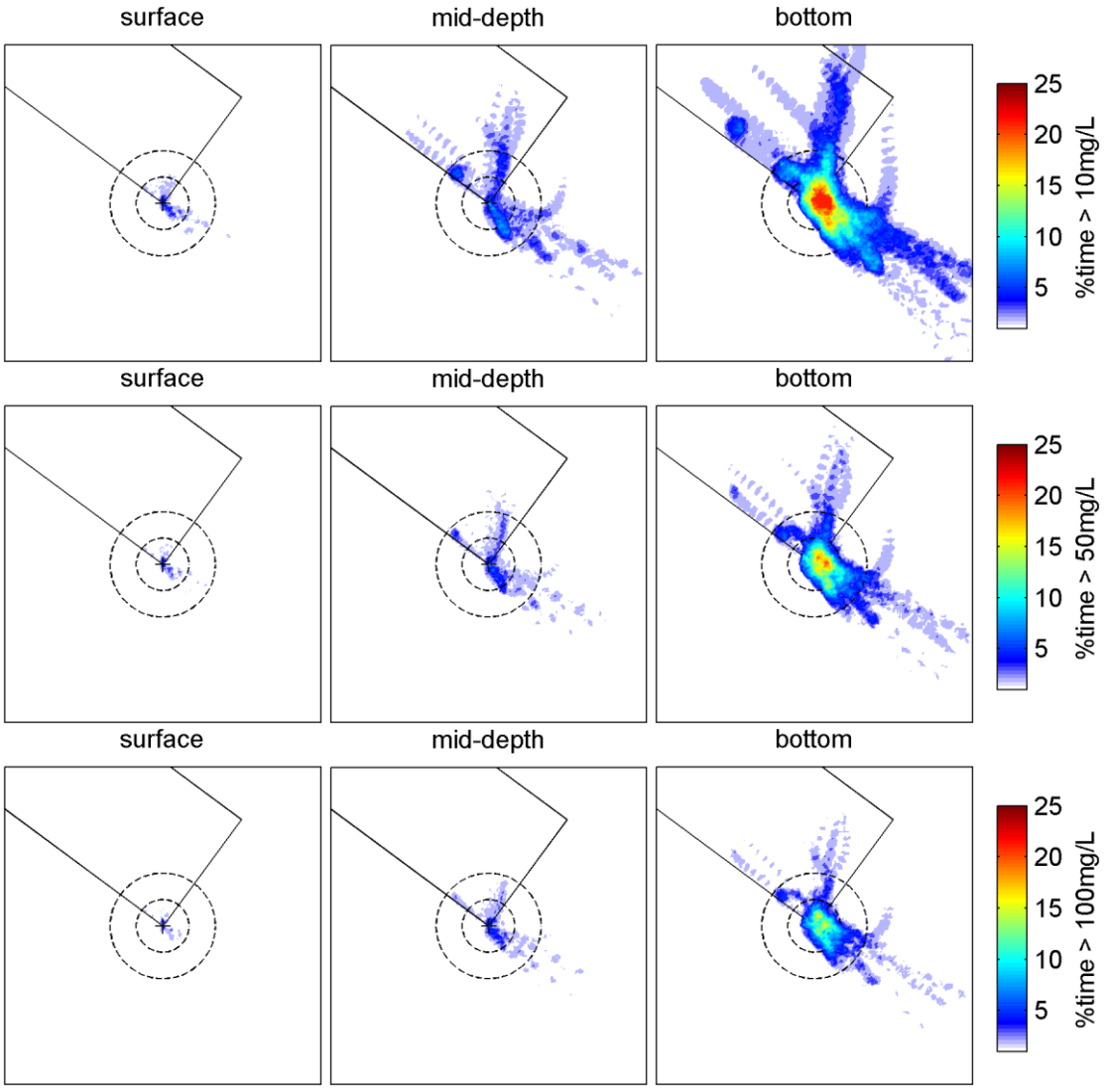

Figure 3.24 Percentage of time *SSC* thresholds of 10, 50, 100 mg.L^{-1} are exceeded during a strong southeast current event, assuming 2-hourly disposal at site 3 with Volvox Asia vessel (V=10,800 m^3). Dashed circles have radiuses of 500 and 1000 m. Background concentrations are of the order 10 mg/L

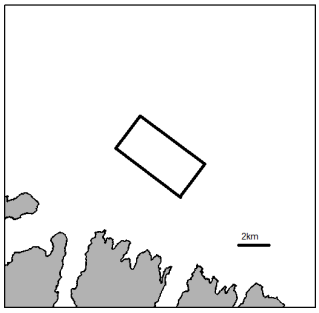

Northeast wind/wave

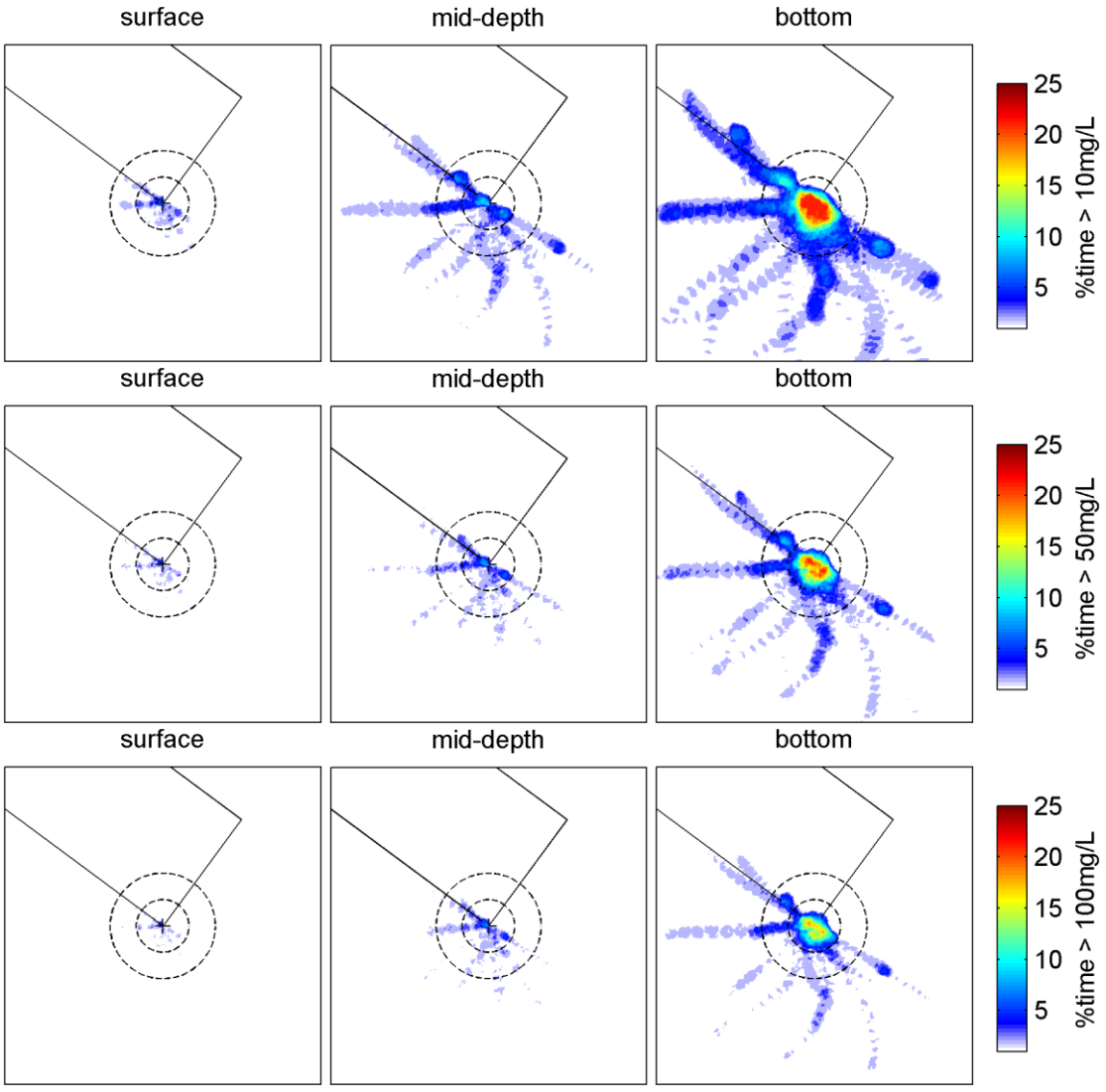

Figure 3.25 Percentage of time *SSC* thresholds of 10, 50, 100 mg.L^{-1} are exceeded during a strong northeast wind/wave event, assuming 2-hourly disposal at site 3 with Volvox Asia vessel (V=10,800 m^3). Dashed circles have radiuses of 500 and 1000 m. Background concentrations are of the order 10 mg/L

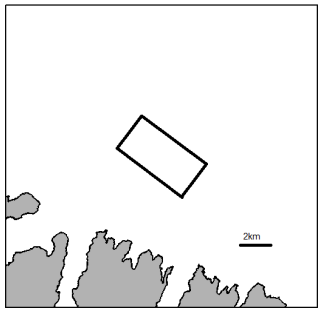

Calm conditions

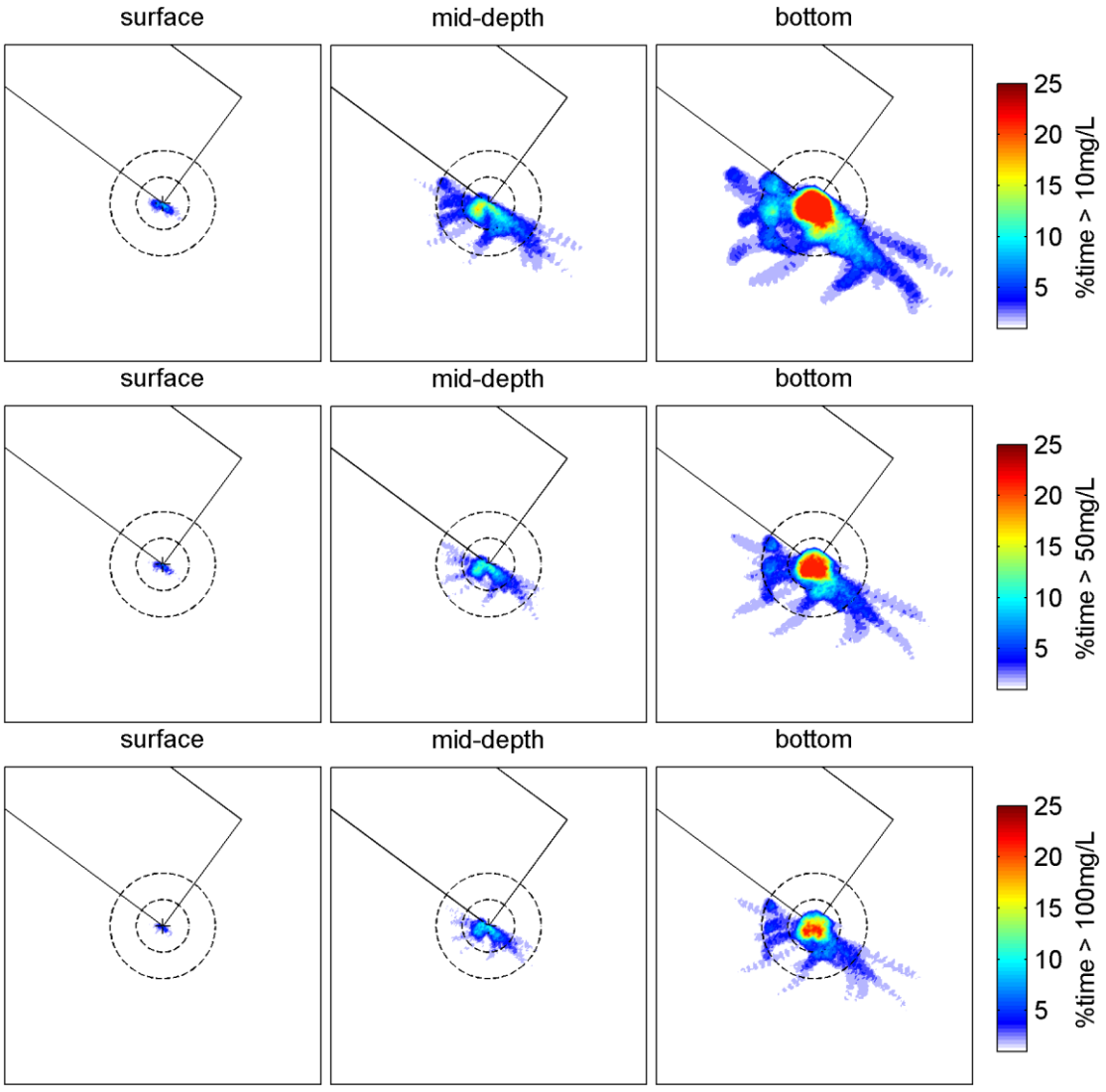

Figure 3.26 Percentage of time *SSC* thresholds of 10, 50, 100 mg.L^{-1} are exceeded during calm conditions, assuming 2-hourly disposal at site 3 with Volvox Asia vessel (V=10,800 m^3). Dashed circles have radiuses of 500 and 1000 m. Background concentrations are of the order 10 mg/L

3.4. Extreme particle dispersion footprints

The results of the particle tracking simulations can be used to estimate the extreme particle dispersions footprints. These footprints are defined by determining the individual particle distances from the release point and then defining a range of distance statistics, notably the extreme excursions such as the 90th, 95th, and 99th percentiles distances. These extreme excursion distances are used to define a polygon around the release location (convex hull) which spatially defines the extreme particle dispersion and worst-case scenarios of plume dispersion. Maximum distances are not included to avoid irrelevant polygon skewness due to individual outliers.

Actual plume *SSC* levels are expected to quickly decrease away from the initial release point, with effective *SSC* levels near the extreme footprint edges being well below ambient levels.

The extreme dispersion footprints for disposal at the centre of the disposal ground (site 5) and southeast corner (site 3) are presented in Figure 3.27. The extreme excursion footprints have elliptic shape elongated in the direction northwest-southeast, consistent with previous results (see Section 3.2.1).

Extreme particle excursions from release position are of the order of 2 km for the mid water plume and 4 km for the bottom plume. These polygons stay well off the coast even for a disposal occurring at southeast corner of the disposal ground (closest point to the coastline). Associated results for the sediment deposition are shown in Figure 3.30.

Convex hull excursion polygons considering discharges from all 5 sites examined within the disposal ground (Figure 1.1, Table 2.1) provide a summary of the absolute extreme dispersion footprint.

Results are presented in Figure 3.29 and Figure 3.30 for the SSC plumes and sediment deposition respectively. The combined extreme dispersion footprints expectedly reproduce an elliptic shape elongated in the northwest-southeast axis. The results indicate no connection of the extreme footprints with any of the closest coastlines and bays, with extreme excursion polygons remaining 1 to 2 km off the closest coast point at all time.

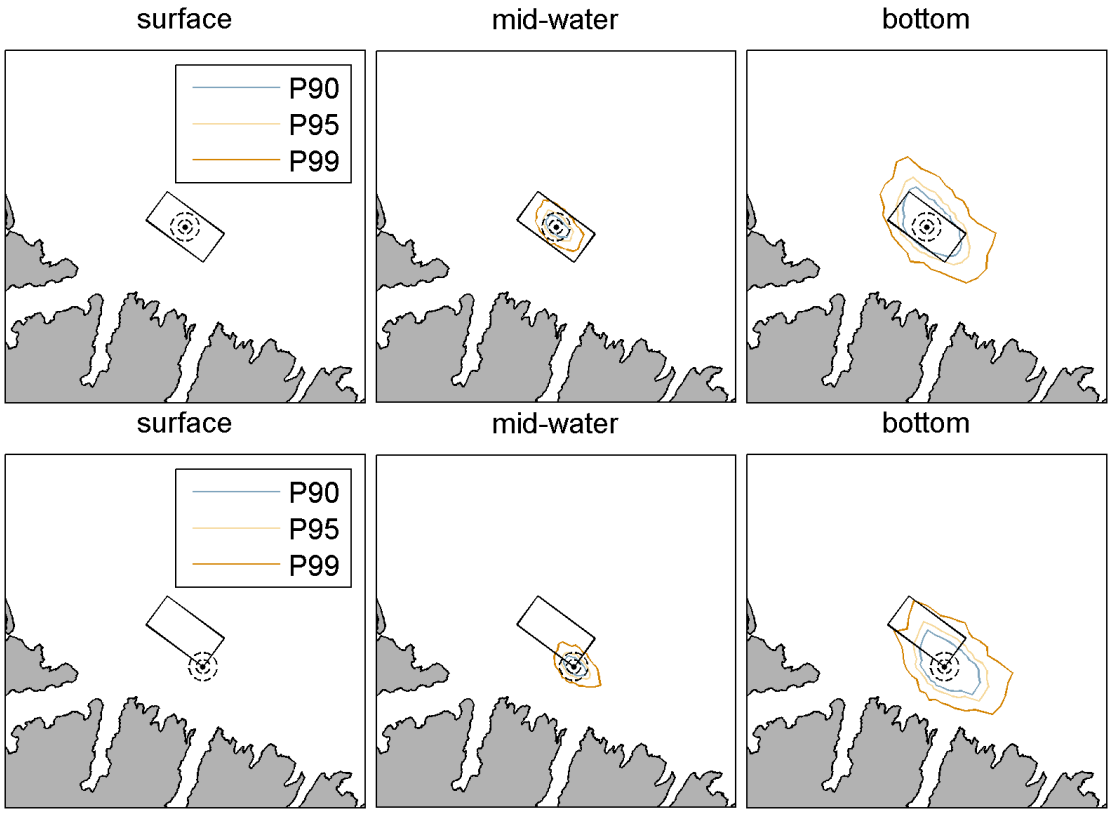

Figure 3.27 Comparison of extreme excursion footprints of SSC plumes resulting from sediment disposal at site 5 (top) and 3 (bottom), for Volvox Asia vessel (V=10,800 m^3), on the surface, mid water and bottom layers of the water column. These results are derived from the 10 year hindcast simulations. Dashed circles have radiuses of 500 and 1000 m.

Figure 3.28 Comparison of extreme excursion footprints of sediment deposition resulting from sediment disposal at site 5 (left) and 3 (right), for Volvox Asia vessel (V=10,800 m^3). These results are derived from the 10 year hindcast simulations. Dashed circles have radiuses of 500 and 1000 m.

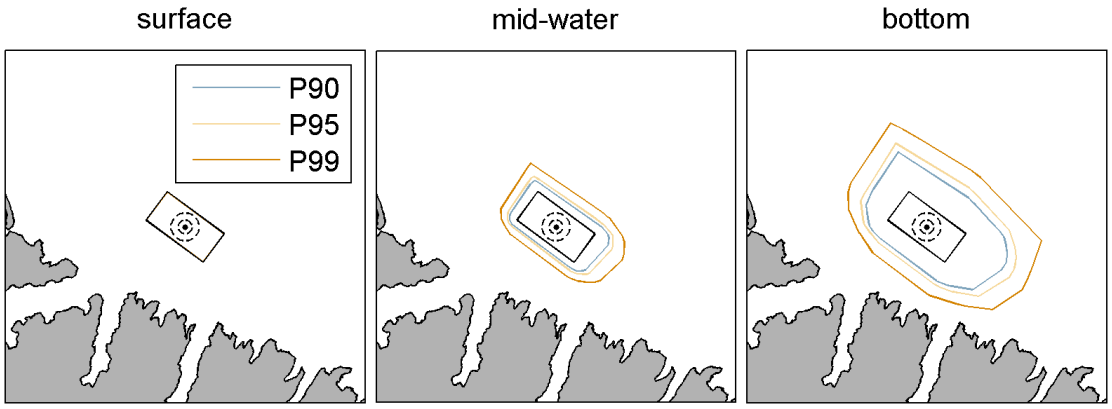

Figure 3.29 Combined extreme excursion footprints of SSC plumes resulting from sediment disposal at the ground corners, for Volvox Asia vessel (V=10,800 m^3), on the surface, mid water and bottom layers of the water column. These results are derived from the 10 year hindcast simulations. Dashed circles have radiuses of 500 and 1000 m.

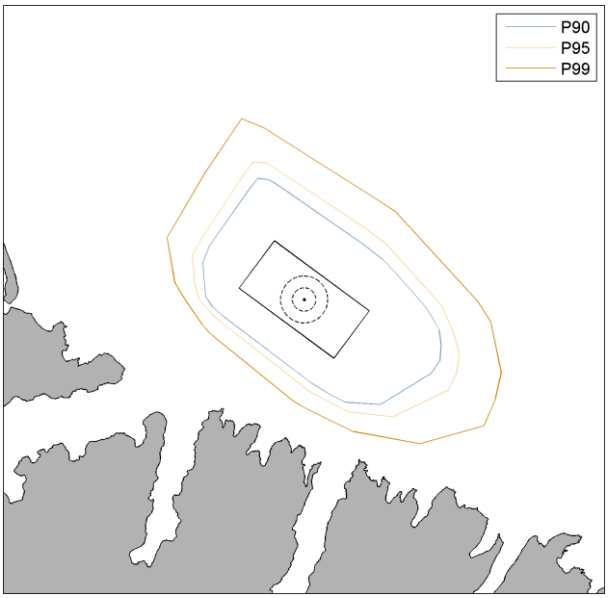

Figure 3.30 Combined extreme excursion footprints of sediment deposition resulting from sediment disposal at the ground corners, for Volvox Asia vessel (V=10,800 m^3). These results are derived from the 10 year hindcast simulations. Dashed circles have radiuses of 500 and 1000 m.

4. SUMMARY

In the context of the proposed CDP at Lyttelton Port Company, the present study assesses the dispersion characteristics of the passive plume associated with the disposal of dredged sediment at an offshore disposal ground in Pegasus Bay.

The passive disposal plume dispersion was simulated with a Lagrangian particle-tracking model and a validated high-resolution hindcast of the Pegasus Bay hydrodynamics. The suspension of sediment in the water column during the sediment disposal, eventually forming the passive plume, was assumed to be the results of two main source terms, namely de-entrainment of sediment into the water column during sediment descent (as a density driven jet) and sediment suspension due to the density current formed following sediment load impact on the seabed. A degree of conservatism was introduced by considering an additional sediment source for possible loss in the near surface layer during disposal operations.

The general dynamics of the plume dispersion were firstly investigated based on a range of short-term simulations of events during hydrodynamic and atmospheric forcing conditions considered to be representative of the expected range at the disposal site.

To derive robust statistical estimations of the plume dispersion and deposition, a second approach consisting of running long-term simulations of disposal activities (10 years) within the historical context was undertaken in order to capture natural variability of the forcing conditions at the site

In addition, estimations of the suspended sediment concentration (*SSC)* exceedance times with respect to several relevant thresholds relating to the ambient level present in Pegasus Bay were made.

The key findings of the study are summarized below:

- The most significant *SSC* levels are found in the bottom layer due to sediment suspension by the density current formed following sediment load impact, and are contained within a 300 m radius from the release position. Sediment settling is rapid given the proximity of the seabed. Surface and mid water *SSC* plumes are dispersed for longer period but have limited spatial extents and *SSC* levels (relating to the expected percentage of sediment entering the passive plume at these levels).

- Mean *SSC* derived from the 10-year plume hindcast of sediment disposal indicates elliptic plume patterns with the major axis consistent with the northwest-southeast direction of the dominant ambient currents. A slight skewness (i.e. asymmetry) to the southeast can be present which is consistent with the expected residual current.

- In the bottom layer, the 10 $mg.L^{-1}$ contour line generally stays within 1 km of the disposal location and within 500 m in the mid-water layer. In the surface layer, *SSC* plumes are very limited, with typical magnitudes below 10 $mg.L^{-1}$.

- Patterns of the mean sediment deposition fields associated with the passive plume have an elliptic pattern with the major axis directed northwest-southeast, with a slight skewness to the southeast. The mean deposition thickness field resulting from the disposal of the passive plume component of one hopper load indicates that the 1 mm contour line typically remains within a radius of 500 m from the discharge position.

- The *SSC* plumes and deposition footprints remain 2 to 3 km from the nearest shoreline point, even when sediment is disposed on the southernmost disposal ground corner (i.e. point closest to the coast in the disposal ground).

- Suspended sediment concentration exceedance times relative to specific thresholds relating to the approximate mean ambient concentration naturally occurring in Pegasus Bay, and slightly elevated levels (10, 50 and 100 $mg.L^{-1}$) have been estimated. These values are several orders of magnitude less than the estimated average surface water *SSC* at the mouth of the Waimakariri River (estimated to be an average *SSC* of 1400 $mg.L^{-1}$).

- On average, the 10 $mg.L^{-1}$ threshold is exceeded 10 to 20 % of the time in the bottom layer within a radius of ~300 m from the discharge site. In the mid-water level, exceedances of up to 5 % are contained within a 500 m radius and become insignificant past the 1 km radius. The largest *SSC* threshold of 100 $mg.L^{-1}$ is typically exceeded 5-10 % of the time within 100 - 200 m from the release position in the bottom layer but very rarely in the mid water and surface levels.

- Similar *SSC* exceedance times were also estimated during the shorter-term representative events. These indicates that the considered *SSC* levels can be exceeded more frequently (up to ~20-25% in the bottom layer) due to either dispersion of the plume in a predominant direction (e.g. following a strong current) or limited ambient potential for dispersion (e.g. very calm weather periods).

- Extreme particle dispersion footprints associated with sediment disposal within the proposed ground show no direct impingement of the shoreline.

REFERENCES

Haidvogel, D.B., Arango, H.G., Hedstrom, K., Beckmann, A., Malanotte-Rizzoli, P., Shchepetkin, A.F., 2000. Model Evaluation Experiments in the North Atlantic Basin: Simulations in Non-linear Terrain-Following Coordinates. Dyn. Atmosphere Oceans 32, 239–281.

Madarasz, A., 2006. Nearshore Coastal Water Quality in Hawke's Bay. Hawke's Bay Regional Council.

Mulder, T., Syvitski, J.P.., 1995. Turbidity Currents Generated at River Mouths during Exceptional Discharges to the Worlds Oceans. J. Geol. 103, 285–299.

Pinkerton, M., Schwarz, J., Gall, M., Beaumont, J., 2013. Satellite ocean-colour remote sensing of the South Taranaki Bight from 2002 to 2012. Prepared for Trans-Tasman Resources Ltd.

Soutelino, R.G., Beamsley, B., 2015. The influence of the Southland Current on circulation patterns within Pegasus Bay. Presented at the Coasts and Ports, Beamsley, p. 7.

Spearman, J., Bray, R.N., Land, J., Burt, T.N., Mead, C.T., Scott, D., 2007. Estuarine and Coastal Fin Sediments Dyanmics.

Vitali, L., Monforti, F., Bellasio, R., Bianconi, R., Sachero, V., Mosca, S., Zanini, G., 2006. Validation of a Lagrangian dispersion model implementing different kernel methods for density reconstruction. Atmos. Environ. 40, 8020–8033.

Zhou, D., 2012. Retrieval of suspended sediment concentration in near-shore coastal waters using MODIS data (D Phil Earth Sciences). Massey University, Palmerston North, New Zealand.